Paleoenvironmental evolution of South Asia and its link to Himalayan uplift and climatic change since the late Eocene

Zehua Song, Shiming Wan, Christophe Colin, Zhaojie Yu, Sidonie Révillon, Hualong Jin, Jin Zhang, Debo Zhao, Xuefa Shi, Anchun Li

Version of Record: https://www.sciencedirect.com/science/article/pii/S0921818121000448
Manuscript_76a89265f86871da59372e821ba2c583

Paleoenvironmental evolution of South Asia and its link to Himalayan uplift and climatic change since the late Eocene

Zehua Song[a,c], Shiming Wan[a,b]*, Christophe Colin[d]*, Zhaojie Yu[a], Sidonie Révillon[e], Hualong Jin[a,c], Jin Zhang[a], Debo Zhao[a], Xuefa Shi[b,f], Anchun Li[a]

[a] Key Laboratory of Marine Geology and Environment, Institute of Oceanology, Chinese Academy of Sciences, Qingdao 266071, China

[b] Laboratory for Marine Geology, Qingdao National Laboratory for Marine Science and Technology, Qingdao 266061, China

[c] University of Chinese Academy of Sciences, Beijing 100049, China

[d] Université Paris-Saclay, CNRS, GEOPS, 91405, Orsay, France

[e] SEDISOR/UMR6538 "Domaines Oceaniques", IUEM, Place Nicolas Copernic, 29280, Plouzane, France

[f] Key Laboratory of Marine Sedimentology and Environmental Geology, First Institute of Oceanography, SOA, Qingdao 266061, China

* Corresponding author.
E-mail address: wanshiming@ms.qdio.ac.cn (S. Wan); christophe.colin@universite-paris-saclay.fr (C. Colin)

Abstract

Reconstructing the Cenozoic sedimentary history of the Bay of Bengal (BoB) is significant for understanding the evolutionary history of South Asian river systems and the links between river development, tectonic deformation and global climate change. Here, we present the first long-term clay mineral record combined with Sr-Nd isotopic compositions from a 200-m-long sediment core from Ocean Drilling Program (ODP) Site 758 in the southern BoB to establish past variations in sediment sources and river evolution that have occurred since the late Eocene. Provenance analysis suggests that the contribution of the Himalayan source materials from the Irrawaddy and Brahmaputra Rivers to the study site became more important and stable since 22 Ma and 8 Ma, respectively. This new evidence indicates that the Brahmaputra and Irrawaddy Rivers were possibly initiated in the early Miocene (~22 Ma). Considering the timing of major tectonic and climatic evolution in South Asia, we conclude that the two phases of tectonic uplift of the Himalayan orogen that occurred in the early and late Miocene were the primary controls on river development in South Asia and provenance changes in the southern BoB. Global cooling and Indian drying after the late Miocene could also have strengthened Himalayan erosion and contributed more illite and chlorite to the South Asian margin.

Keywords: River evolution; Himalayan uplift; Clay minerals; Sr-Nd isotopes; Provenance; Bay of Bengal; Ocean Drilling Program

1. Introduction

The elevation and topography of the Himalaya-Tibetan Plateau (HTP) were essentially driven by collisions between the Indian and Asian continents during the Eocene (ca. 50 Ma) and their continued convergence thereafter (Harris, 2006). HTP uplift and the resulting deformation of Asian topography in the Cenozoic had a profound influence on the formation and development of Asian drainage systems, as well as the Asian monsoon (Clift et al., 2014; Molnar et al., 1993; Wang, 2004; Zheng et al., 2020). For example, surface uplift in eastern Tibet was considered as the primary cause for the continental-scale drainage configuration and birth of the modern Yangtze River (Zheng et al., 2013), Pearl River (Cao et al., 2018) and Red River (Clift et al., 2006) during the early Miocene (~23 Ma). Moreover, the global climate experienced gradual cooling beginning in the Eocene (Zachos et al., 2001), and paleoenvironmental conditions in Asia shifted from a planetary-wind-dominant type to a monsoon-dominant type in approximately the late Oligocene-early Miocene (ca. 23 Ma) (Guo et al., 2008; Sun and Wang, 2005), whereas the Indian monsoon initiated approximately 9–8 Ma ago (Kroon et al., 1991) or during the Eocene (Licht et al., 2014). The uplift of the HTP that began in the Eocene has played a significant role in strengthening the Asian monsoon and changing the global climate (An et al., 2001; Clift et al., 2014; Prell and Kutzbach, 1992). The interplay of erosion, climate and tectonics during mountain building has attracted much attention for several decades (Clift et al., 2008; Molnar and England, 1990; Raymo and Ruddiman, 1992; Tada et al., 2016). Modern observations and theoretical analyses suggest that large mountain

ranges with high relief that formed through tectonic uplift have significantly higher rates of erosion, as the general relief determines the potential erosive power of runoff (Clark et al., 2004). Climate, as represented by temperature and precipitation, has in turn been identified as a critical factor influencing physical erosion and chemical weathering (White and Blum, 1995). The HTP uplift-induced increase in physical and chemical weathering and consumption of atmospheric CO_2 may have caused the Cenozoic climatic deterioration (Raymo and Ruddiman, 1992). However, this interaction between tectonics and paleoenvironmental evolution in the geological past remains unclear (Misra and Froelich, 2012), largely due to the lack of a continuous long-term sedimentary record that can precisely define the timing of major tectonic and climatic events in the Himalayan region during the Cenozoic (Lenard et al., 2020; Willenbring and von Blanckenburg, 2010). Unfortunately, such direct records are rare within the orogen or immediate hinterland, as the available records are mostly from the Neogene period, and very limited records are from the Paleogene (Awasthi and Ray, 2020; Clift and Webb, 2018).

In contrast, marine deposits on the continental margin of South Asia are generally more continuous and easier to date at higher resolution by biostratigraphy and paleomagnetism. The Bay of Bengal (BoB), as the major sediment sink for South Asian rivers draining through the HTP, has excellent preserved erosional records of its source region (France-Lanord et al., 2014; McNeill et al., 2017). Chemical weathering strongly affects the element geochemistry and clay mineral assemblages of siliciclastic sediments (Clift et al., 2014; Colin et al., 1999; Nesbitt and Grant M.

Young, 1996; Wan et al., 2012a). Such geochemical or mineralogical signatures ultimately leave traces in offshore sedimentary records (Clift et al., 2008; Galy et al., 2010; Wan et al., 2017; Zhang et al., 2019). Sedimentation in the Bengal Fan began at least 40 Ma ago and has built the world's largest active submarine mega-fan (Curray et al., 2002). The BoB thus provides an excellent record of Himalayan erosion and weathering, which is related to the evolution of the South Asian river system and thus the tectonic uplift of the HTP over a million-year timescale (France-Lanord and Derry, 1997; France-Lanord et al., 2014). There are some HTP erosion-related long-term sedimentological, mineralogical and geochemical records from the BOB, including records from the Deep Sea Drilling Project (DSDP) Site 218 (12 Ma) (Galy et al., 2010), Ocean Drilling Program (ODP) Site 718 (17 Ma) (Derry and France-Lanord, 1996), and Integrated Ocean Drilling Program (IODP) Sites U1447 (10 Ma) (Lee et al., 2020) and U1480 (22.5 Ma) (Pickering et al., 2020). However, very few long-term and continuous sedimentary records are able to extend to the early Miocene-Eocene, during which the HTP region experienced significant tectonic uplift (Clift and Webb, 2018; Ding et al., 2017) and related drainage reorganization. Therefore, recovering a pre-Miocene erosional record is the key to improving our understanding of the evolution of South Asian river systems and its possible link to HTP uplift (Awasthi and Ray, 2020).

In this study, we present a continuous record of clay mineral assemblages combined with Sr-Nd isotopic compositions of the clay-sized fraction (<2 μm) of sediments at ODP Site 758 in the southern BoB from approximately 37 Ma. Here, we

address this long-term sediment record to (1) constrain the variation in sedimentary sources of clay minerals since the late Eocene and (2) reconstruct the South Asian paleoenvironmental evolution history and thus assess its possible links to tectonic uplift of the Himalayan region and climate change in the Cenozoic.

2. Geological setting

2.1. The Himalaya and South Asian rivers

The history of HTP uplift remains controversial (Clift and Webb, 2018; Ding et al., 2017), although more studies tend to support its phased uplift following the India–Asia collision (Tapponnier et al., 2001; Wang et al., 2014). The first pulse of uplift in the southern and central Tibetan Plateau occurred during the late Eocene (~40 Ma), soon after the "hard" collision of India and Eurasia at ~45 Ma (Dai et al., 2012; Hoke et al., 2014; Polissar et al., 2009; Rowley and Currie, 2006; Tada et al., 2016; Wang et al., 2008). A second pulse of surface uplift occurred between 25 and 20 Ma in the northeastern, northwestern, and central Tibetan Plateau and the Pamir Plateau (Amidon and Hynek, 2010; George et al., 2001; Lease et al., 2011; Sobel and Dumitru, 1997; Xiao et al., 2012; Zhang et al., 2011). A third pulse of uplift occurred at approximately 15–10 Ma when the Tibetan Plateau expanded toward the north and east to attain a width and altitude close to its present configuration (Hough et al., 2011; Yuan et al., 2013). After ~10 Ma, the uplift continued in the northeastern part of the Tibetan Plateau, but it was not as significant as previously thought, whereas

progressive southward migration of the zone of greatest rock uplift occurred in the frontal Himalaya at that time (Deeken et al., 2011; Tada et al., 2016).

Cenozoic drainage variations around the BoB that have occurred since the India-Asia collision remain unclear because of the complexity of regional tectonic evolution and sparse long-term and continuous weathering records (Licht et al., 2016; P. Zhang et al., 2019). Researchers have suggested that the Yarlung Tsangpo River (the upper reach of the Brahmaputra River) and Irrawaddy River were tributaries to the Red River before the onset of the Himalayan collision (Clark et al., 2004). Moreover, detrital zircon records from the Red River have demonstrated that there was no connection between the Irrawaddy River and Red River after the late Miocene (Hoang et al., 2009). Plate reconstruction has indicated that the Irrawaddy River was possibly initiated during the mid-Oligocene due to the rise of the Indo-Burman Ranges, whereas both the Ganges-Brahmaputra (G-B) river system and Irrawaddy River have maintained a stable paleodrainage pattern since the early Miocene because of critical uplift of the HTP (Zhang et al., 2019 and reference therein). Other prospective studies indicate that a Yarlung Tsangpo-Irrawaddy system existed from the late Eocene to its collapse in the early Miocene (Robinson et al., 2014), which was coincident with deformation along the strike slip Jiali-Parlung and Gaoligong strike-slip faults in the eastern syntaxis (Lin et al., 2009) and the Sagaing fault in Myanmar (Mitchell et al., 2007). However, a comprehensive evaluation of tectonics' control on river evolution is impossible without reliable offshore sediment records.

2.2. The Bay of Bengal

The BoB is the largest deep-sea fan in terms of sedimentary volume and receives a large amount of sediment flux derived from the Himalayan river system (G-B river system and Irrawaddy River) and small rivers from the Indian continent (i.e., the Mahanadi, Godavari, and Krishna Rivers). Subduction along this zone likely started at approximately 98 Ma (Bhattacharya et al., 2020). The BoB was formed during the collision of the Indian subcontinent with the southern margin of Asia. This collision has started in the middle Paleocene (ca. 59 Ma) (Hu et al., 2016) and created an indentation in Asia in which India lies today (Curray, 2014). During this long collision process, the western Sunda Arc was deformed and rotated from the postulated precollision alignment into its present location: the Sunda Arc's plate edge to the eastern Himalayan syntaxis, the Himalayan front to the western Himalayan syntaxis, and the southern part down through Pakistan to the Arabian Sea (Curray, 2014). Bangladesh occupies most of the Bengal Basin, which contains the Bengal Delta (sometimes called the Ganges–Brahmaputra Delta);this delta may be the largest delta in the world. The sedimentary fill in the Bengal Fan and the Bengal Delta, which exceeds 20 km, is currently derived primarily from erosion of the HTP, and has been derived from this source since at least the middle Eocene, approximately 43 to 50 Ma (Curray, 2014). The sedimentary part of the fan is subdivided into three sections by seismic stratigraphy of two unconformities within lower Eocene and upper Miocene strata, which are postulated to be the time of first deposition within the fan and the onset of the diffuse plate edge or intraplate deformation in the southern or lower fan,

respectively (Curray et al., 2002).

3. Material and Methods

ODP Site 758 (5°23.05'N, 90°21.67'E) is located in the southern BoB on the Ninetyeast Ridge at a water depth of 2925 m, which is approximately 1000 m above the Bengal Fan; this site permits a continuous sedimentary record without turbidite deposits (Fig. 1a). The sediments at this site consist mainly of biogenic pelagic calcium carbonate ooze with minor amounts of terrigenous silt, clay and volcanic tephra (Farrell and Janecek, 1991). For this study, we investigated the upper 249 m of core 758A, which spans from the late Eocene to the Holocene. The lithology of the studied interval can be divided into two major units according to sediment composition: Unit I (0-122 m; Holocene to middle Miocene) is dominated by nannofossil ooze with clay and foraminifers; Unit II (122-249 m; middle Miocene to late Eocene) is characterized by nannofossil and calcareous nannofossil chalk (Pierce et al., 1989). A total of 93 samples were sampled at a mean interval depth of approximately 2.67 m, and no ash/tephra layers were included. All the samples were measured for their clay mineral assemblages, and 18 samples were selected for the analysis of the Sr and Nd isotopic compositions within the clay-sized silicate fraction.

The age model of the ODP Site 758 was established on the basis of biostratigraphy of calcareous nannofossils and diatoms with 20 age controls obtained on board using the most recent dates of the magnetic reversals with linear interpolation between control points (Pierce et al., 1989) (Fig. 2). The sediment sequences span the last 37

Ma, with a mean sample resolution of approximately 400 ky.

The weight percent of total terrigenous materials in bulk samples was determined, and the total mass accumulation rate (MAR) (g/cm^2/ky) was calculated according to the method of Rea and Janecek (1981). On the basis of the data of LSR and DBD data provided by Banerjee et al. (2017) and Pierce et al. (1989), the total MAR values were calculated, and in turn, the MAR of terrigenous materials was determined by multiplying the total MAR by the weight percent value of the individual components. Using these accumulation rates, dilution effects by other components were excluded, and furthermore, burial-related sediment compaction was corrected (Rea and Janecek, 1981).

Clay mineral studies of 93 samples from ODP Site 758 were carried out on the <2 μm fraction, which was separated using Stoke's settling velocity principle and recovered by centrifuging (Wan et al., 2012b) after removal of organic and carbonate matter by treatment with H_2O_2 (15%) and HCl (0.5 mol/L), respectively. Clay minerals were identified by X-ray diffraction (XRD) using a D8 ADVANCE diffractometer at the IOCAS laboratory with routine XRD analysis (Wan et al., 2012b). Semiquantitative estimates of peak areas of the basal reflection for the main clay mineral groups (smectite – 15-17 Å, illite – 10 Å, and kaolinite/chlorite – 7 Å) from ethylene glycol curves by Topas 2P software using the empirical factors of Biscaye (1965). Replicate analysis of the same sample produced a result with a relative uncertainty below 5%. Additionally, the illite chemistry index was estimated using the ratio of the 5 Å and 10 Å illite peak areas. Ratios of the illite chemistry index higher than 0.4 represent Al-rich

illite, which is formed under strong hydrolysis, and ratios lower than 0.4 indicate Fe-Mg-rich illite that is characteristic of weak chemical weathering conditions. Illite and smectite crystallinity was calculated as the full width at half maximum (FWHM) height of the illite peak (10 Å) and smectite peak (17 Å), respectively. The results are shown in Table 1.

The Sr-Nd isotopic compositions of the clay-sized silicate fraction were determined on 18 samples. The clay-sized fraction of all samples was leached and separated using the same procedure as the procedure for the clay mineral analysis before isotope analysis. Approximately 100 mg of sample was weighed and dissolved in a mixture of ultrapure HNO_3 + HF + $HClO_4$. Sr and Nd fractions were separated using standard ion exchange techniques (Révillon et al., 2011; Shen et al., 2017). Sr and Nd isotopic compositions were measured in static mode on a Thermo TRITON at the SEDISOR in Plouzane, France. All measured Sr and Nd ratios were normalized to $^{86}Sr/^{88}Sr = 0.1194$ and $^{146}Nd/^{144}Nd = 0.7219$, respectively. During the analysis, the Sr isotopic compositions of standard NBS-987 gave $^{87}Sr/^{86}Sr=0.710259\pm7$ (n=9, recommended value 0.710250); Nd standard La Jolla gave 0.511852±2 (n=3, recommend value 0.511850) and standard JNdi gave 0.512102±6 (n=3, recommended value 0.512100) (Révillon et al., 2011).

4. Results

4.1. Terrigenous MAR and clay mineralogy

The terrigenous MAR at ODP Site 758 varies between 0.01 to 0.89 g/cm^2/ky, with an average of 0.32 g/cm^2/ky. In general, the terrigenous MAR was very low and relatively stable between 37 and 8.5 Ma, except for a high interval between 27 to 20 Ma, and rapidly increased after approximatel 8.5 Ma (Fig. 2).

Downcore variations in clay mineral assemblages at ODP Site 758 are shown in Fig. 2. The assemblages are dominated by smectite (14–94%) and illite (2–58%), while kaolinite (1–28%) and chlorite (0–14%) are less abundant (Table 1). In general, both illite and chlorite remained relatively stable between 37 and 8 Ma, and rapidly increased after ~8 Ma and then rapidly decreased after 3.5 Ma, while the opposite tendency occurred with smectite. In contrast, the kaolinite content varied, and relatively high contents were present between 35–10 Ma (from 11 to 28%), and then the content decreased discontinuously to an average of 13% with two time intervals of lower percentages occurred from 9.5 to 8 Ma and from 3.5 to 0 Ma.

The illite chemistry index of all samples at ODP Site 758 varies between 0.02 and 0.40, with an average of 0.21, suggesting that illite is typically rich in Fe–Mg and was formed in an environment dominated by strong physical erosion and weak chemical weathering. The crystallinities of illite and smectite vary between 0.16–0.75°Δ2θ (average of 0.33°Δ2θ) and 0.92–2.16°Δ2θ (average of 1.31°Δ2θ), respectively. In general, the illite chemical index is lower with large oscillations between 37 and 8 Ma and it increased after approximately 8 Ma, whereas the

crystallinity of illite and smectite have an approximately contrasting pattern (Fig. 2).

4.2. Sr-Nd isotopic compositions

The Sr–Nd isotopic compositions of the terrigenous clay-size fractions from ODP Site 758 and the potential sedimentary sources to the BoB are reported in Table 2. At ODP Site 758, $^{87}Sr/^{86}Sr$ ratios vary between 0.711 and 0.722 with a mean value of 0.717, and εNd ranges from -16.5 to -9.9 with a mean value of -12.5.

In general, the $^{87}Sr/^{86}Sr$ values of the clay-sized fraction at Site 758 display a long-term increasing trend after 37 Ma but are punctuated with a temporary decrease between 13 and 8 Ma (Fig. 2). εNd displays a decreasing trend from 37 to 22 Ma, and becomes less radiogenic between 22 and 8 Ma and then slightly reverses to more negative values after ~8 Ma.

5. Discussion

5.1. Potential sediment sources

A prerequisite for the interpretation of mineralogical and geochemical records in marine sediments is knowledge of the potential source areas, as well as the history of sediment transport processes (Colin et al., 2006; Zhao et al., 2017). The BoB has multiple potential sediment sources, including the G-B river system, rivers from the Indo-Burman Range volcanic province and the east Himalaya, and rivers from the Deccan Traps volcanic province, Sibumasu Block rocks and the Peninsular gneissic

rocks. As there has been no systematic past reconstruction of mineralogical and geochemical signatures of potential rivers feeding the BoB, we need to assume that mineralogical and geochemical compositions remained similar in the geological past (Clift et al., 2014; Derry and France-Lanord, 1996; Wan et al., 2007). Nevertheless, clay mineralogy combined with Sr-Nd isotopic compositions of marine sediments from the BoB is suitable to establish the main sedimentary sources derived from the Himalayan region because the sources are characterized by contrasting mineralogical and geochemical signatures (Colin et al., 1999, 2006; Derry and France-Lanord, 1996; France-Lanord et al., 1993; Joussain et al., 2016; Lupker et al., 2013; Tripathy et al., 2014).

Fine-grained suspended sediments from the Himalayan river system and other Indian rivers can be transported to the deep sea by surface currents (Gourlan et al., 2008; Joussain et al., 2016; Li et al., 2017; Lupker et al., 2013). The surface currents in the BoB are mainly controlled by the Indian monsoon and display seasonal reversal, which shifting from a cyclonic gyre during the winter monsoon to an anticyclonic gyre during the summer monsoon (Kolla et al., 1976; Shankar et al., 2002). Researchers have suggested that the G-B river system was the most significant contributor of sediments to the BoB during the past several million years (Awasthi and Ray, 2020; Derry and France-Lanord, 1996; France-Lanord et al., 1993). At present, the G-B river system, which developed on the southern margin of the Himalayan Range, is still one of the largest sediment discharge supplier in the world. The G-B river system delivers an average of 1060×10^6 t/yr of sediment to the BoB

(Milliman and Farnsworth, 2011) and drains through many kinds of rock types, such as felsic intrusives, Precambrian metamorphics, Paleozoic-Mesozoic sandstones, and shales, and Precambrian-Cambrian shield limestones (Heroy et al., 2003; Huizing, 1971). The Irrawaddy River is the third largest river in this region, with an average sediment discharge of 325×10^6 t/yr. There are many tributaries of the Irrawaddy River that flow through the Mogok metamorphic belt, the Sibumasu block, the central Myanmar forearc basin, the Jade Mines Belt, and the Indo-Burman Ranges, and the basin contains abundant source rock types (Barley et al., 2003; Mitchell et al., 2012, 2007; Stephenson and Marshall, 1984). In addition, minor sediment contributions come from the Indian peninsular rivers and Arakan coastal rivers, with relatively low sediment discharges of 236×10^6 t/yr and 130×10^6 t/yr, respectively (Milliman and Farnsworth, 2011). The Godavari-Krishna river system drains from the Deccan Trap basalts and Precambrian metamorphic rocks (Rao and Kessarkar, 2001).

ODP Site 758 is located on the Ninetyeast Ridge between the Bengal Fan and the Nicobar Fan and thus excludes the significant influence of turbidity transport from the G-B river system and/or Irrawaddy River. Previous studies have suggested that sediments deposited on the Ninetyeast Ridge mainly originated from terrigenous material eroded from the HTP and Indian subcontinent (Zhang, 2002). However, paleogeographic reconstruction suggests that the location of our study site and the Indian subcontinent were far from the subduction front during the Eocene-Oligocene (Zhang et al., 2017), so the sediment contributions from the potential sources should vary over geological time as a function of paleogeography (Awasthi and Ray, 2020).

Until now, the oldest offshore record of weathering and erosion of the HTP was from Site 718 of ODP Leg 116 of the southern BoB (Fig. 1), which was dated to approximately 17 Ma (Derry and France-Lanord, 1996). Consequently, mineralogy and the Sr-Nd isotopic composition characteristics of the clay-sized silicate fraction of the ODP Site 758 could provide a longer and continuous history of sediment provenance variation on the Ninetyeast Ridge over the last 37 Ma. Here we constrain the provenance of Site 758 by comparing its clay mineralogy and Sr-Nd isotopic compositions with potential sources in the context of paleogeographic evolution.

5.2. Clay mineral constraints on provenance

Clay mineral assemblages in marine sediments can be used as potential proxies to distinguish clay-sized sediment provenance (Biscaye, 1965; Wan et al., 2012b) as well as the environmental conditions (climatic conditions) of sedimentary sources (Wan et al., 2017). Previous studies have shown that clay minerals transported to the BoB originate mainly from the Himalayas, Indo-Burman Range, Deccan Traps and southern Indian continent peninsular gneissic rock (Ahmad et al., 2005; Colin et al., 2006; Derry and France-Lanord, 1996; France-Lanord et al., 1993). We must keep in mind that rivers do not always have a constant clay mineral assemblage, which can vary in response to climatic or tectonic changes in the geological past (Clift et al., 2020; Derry and France-Lanord, 1996; Shen et al., 2017; Wan et al., 2017), although this is very difficult to constrain because of the lack of end-member data that can extends to the late Eocene.

Modern G-B river system sediments consist mainly of illite (average of 58%), with lower amounts of smectite (~15%), kaolinite (~14%) and chlorite (~13%) (Khan et al., 2019; Sarin et al., 1989), due to strong physical erosion of the High Himalayan Crystalline Sedimentary Series and/or the Lesser Himalayan Series. In the G-B river system, illite and chlorite are primary minerals and are produced mainly from intensive physical erosion and moderate chemical weathering of metamorphic (i.e., muscovite or biotite) and granitic parent rocks of the high Himalayas (Huyghe et al., 2011; Sarin et al., 1989). In contrast, there are higher concentrations of smectite in riverbank material and in suspended sediments of the Indo-Gangetic floodplain than in the watershed tributaries of the Ganges River (Huyghe et al., 2011; Sarin et al., 1989). This increase in the proportion of smectite in the floodplain may derive from the recycling of smectite-rich Siwalik Group sedimentary rocks, from rivers draining the Deccan Traps (Sarin et al., 1989), and from pedogenesis in the Ganges River plain (Huyghe et al., 2011). Irrawaddy River sediments from the Irrawaddy Delta are dominated by smectite (60%) and kaolinite (20%), while illite (15%) and chlorite (5%) are less abundant (Rodolfo, 1969). Smectite is then likely derived mainly from the Irrawaddy floodplain, but a small contribution from volcanic areas cannot be totally excluded (Colin et al., 2006).

In contrast, rivers originating from the Deccan Traps (Godavari and Krishna Rivers) have higher contents of smectite, as it can be easily produced by chemical weathering of basaltic material. The clay mineral assemblages of the Godavari and Krishna Rivers are characterized by high smectite (~53%) and illite (~22%), while

chlorite (~18%) and kaolinite (~7%) are less abundant (Phillips et al., 2014). Terrigenous sediments from the Indo-Burman Ranges and Andaman-Nicobar Ridge are characterized by basaltic materials and high contents of smectite (average content of 79%) and lower contents of chlorite (~9%), kaolinite (~8%) and illite (~4%) (Ali et al., 2015). The strong chemical weathering of volcanic rocks in wet and humid regions can produce abundant smectite (Chamley, 1989), and basaltic volcanic rocks are indeed widely developed in the Deccan Traps, Indo-Burman Ranges and Nicobar Ridge (Licht et al., 2013). In addition, the Peninsular gneissic rock in the southern Indian continent is under the influence of a humid tropical climate and undergoes intense chemical weathering. The clay mineral compositions of sediments from the southern Indian continent indicate moderate contents of smectite (31%) and illite (30%) with associated kaolinite (25%) and chlorite (15%) (Kessarkar et al., 2003).

To constrain the provenance of clay minerals, we applied a smectite-(illite+chlorite)-kaolinite ternary diagram to show the clay mineralogical results of ODP Site 758 samples for different periods (37-22 Ma, 22-8 Ma and 8-0 Ma) and modern river sediments (Fig. 3a). All the samples at the study site plot as a group subparallel to the (illite+chlorite)-smectite line and range between several potential sedimentary sources. This trend can be interpreted as a mixture of multiple sediment sources from the G-B river system (high illite-chlorite end-member) and Andaman-Nicobar Ridge, Irrawaddy River, Peninsular gneisses and/or Deccan Traps (relatively high smectite end-member). Clay mineral assemblages present a significant change at ~8 Ma with sediments older than 8 Ma, which is consistent with the modern

mineralogical composition of the east Indian rivers and Andaman-Nicobar Ridge where weathering of basaltic volcanic material can produce a high content of smectite content (Awasthi et al., 2014). In contrast, clay mineralogical assemblage sediments younger than 8 Ma plot in the field of the modern G-B river system and Irrawaddy River, where strong physical erosion of the high reliefs in these river basins produces large volumes of illite and chlorite.

Illite and chlorite could then be derived mainly from physical erosion of the highlands of the Himalayan river basins, whereas smectite could be derived from chemical weathering of primary minerals in the Himalayan river system floodplain or from weathering of volcanic rock in the Deccan Traps and Andaman-Nicobar Ridge. Kaolinite is mainly produced by stable chemical weathering, which indicates that kaolinite at the site could be derived from floodplain such as the Indo-Gangetic plain or from weathering under strong hydrolysis conditions on the stable southern Indian continent.

In addition to provenance changes, other offshore processes may also influence the clay mineral assemblage of the sediment within the core, such as oceanic current transport and diagenesis after burial (Chamley, 1989). Although the Indian monsoon may have initiated or strengthened at 7-8 Ma (Kroon et al., 1991; Quade et al., 1989), it seems unlikely that the southwest summer monsoon-driven surface current would have preferentially transported more Himalayan materials to the study site relative to suspended sediment from the Indian Peninsula and/or Andaman-Nicobar Ridge after that time. In addition, the major diagenetic change in clay minerals is the progressive

transformation of smectite to illite, which primarily depends on temperature (Fagel, 2007). In strata with a normal temperature gradient (~30 °C/km), burial diagenesis of clay minerals usually occurs at depths deeper than 2500-3000 m (Chamley, 1989; Fagel, 2007). Both the low temperature gradient (average of 28.2 °C/km) (Sijinkumar et al., 2016) and the shallow burial (<250 m) of sediments on the Ninetyeast Ridge exclude the possible influence of diagenesis on clay minerals.

Therefore, the clay mineral record of ODP Site 758 implies that smectite and kaolinite were weathered from the south Indian subcontinent and Andaman-Nicobar Ridge, whereas illite and chlorite originated mainly from the highlands of the Brahmaputra River, Indo-Burman Range and Irrawaddy River. The significant change in clay mineralogy from smectite-rich to illite/chlorite-rich at the study site after approximately 8 Ma possibly indicates an increased sediment contribution from the Himalayan range with stronger physical erosion at that time.

5.3. Sr-Nd isotope constraints on provenance

In comparison with clay minerals that could be affected by the mineralogy of the parent rock and the intensity of hydrolysis conditions in the soil, εNd value, and to a lesser extent, $^{87}Sr/^{86}Sr$ values, can be used as reliable tracers for identifying the source of sediments in the BoB (Colin et al., 1999; Joussain et al., 2016; Shen et al., 2017; Yu et al., 2020; J. Zhang et al., 2019). The $^{87}Sr/^{86}Sr$ ratios of sediments in the BoB can be affected by grain size, with more radiogenic values in the fine fraction (Joussain et al., 2016), or by the state of chemical weathering of detrital minerals (Clift et al., 2006;

Colin et al., 1999; Yu et al., 2019). In contrast, εNd values are largely unaffected by grain size (Meyer et al., 2011) and chemical weathering processes (Colin et al., 1999, 2006). Consequently, Sr and Nd isotope analyses carried out on the bulk terrigenous fraction could reflect changes in the particle size and mixing proportions of sediment subpopulations derived from different sedimentary sources. We have investigated the Sr-Nd isotopic compositions of the clay-sized (<2 μm) silicate fraction to minimize the influence of grain size (Chen et al., 2007; Zhao et al., 2017). Although a weathering effect on the Sr isotopic composition is still likely (Awasthi et al., 2018; Mokadem et al., 2015; Shen et al., 2017), the discrepancy between the roughly increased $^{87}Sr/^{86}Sr$ ratio at Site 758 (Fig. 2) and the weakened chemical weathering intensity in the Himalaya since the middle Miocene (Clift et al., 2008) excludes this possibility.

The Sr-Nd isotopic compositions of the clay-sized fraction data at ODP Site 758, along with the Sr and Nd isotopic signatures of potential sources, are reported in a εNd versus $^{87}Sr/^{86}Sr$ diagram (Fig. 3b). Because possible variations in the Sr-Nd isotopic compositions of these Himalayan river basins are not available prior to the late Eocene, we assume that each potential source region remains basically stable (Table 2), although the isotopic compositions of Irrawaddy River sediments would have been different in the geological past due to possible drainage reorganization (Awasthi and Ray, 2020; Robinson et al., 2014). The narrow range of εNd and $^{87}Sr/^{86}Sr$ ratios obtained on bulk sediments from ODP Leg 116 of the southern Bengal Fan confirms that this was the case for the G-B river system for at least the last 17 Ma

(France-Lanord et al., 1993). Modern sediments of the Ganges, derived from rocks of the Himalayan Ranges, have high $^{87}Sr/^{86}Sr$ values of 0.748–0.777 and unradiogenic εNd values that vary between -19.1 and -15.7 (Singh et al., 2008), and modern sediments of the Brahmaputra River have $^{87}Sr/^{86}Sr$ values of 0.718–0.734 and unradiogenic εNd values that vary between -16.9 and -12.4 (Singh and France-Lanord, 2002). The Irrawaddy River is characterized by relatively unradiogenic εNd (-9.1 to -11.5) and low $^{87}Sr/^{86}Sr$ end-member values (0.712-0.724) (Colin et al., 1999; Damodararao et al., 2016). The Yarlung-Brahmaputra River flowed through the Lhasa terrane at the boundary between the Indian and Asian crust, while the Irrawaddy River flowed through the Burma terrane and other terrains that drained from the Indo-Burman Ranges. The basement rocks of the Lhasa terrane and nearby Burma terrane have close Sr and Nd isotope characteristics and are believed to be the main suppliers of the Brahmaputra River and Irrawaddy River, respectively (Licht et al., 2013). Modern sediments of the Godavari and Krishna Rivers on the east Indian continent have $^{87}Sr/^{86}Sr$ values ranging from 0.720-0.730 and εNd values that vary between -18.2 and -12.0 (Ahmad et al., 2009). Rocks of the Sibumasu (Shan-Thai) block, which is located at east of the west Burma block, have low $^{87}Sr/^{86}Sr$ values (0.704-0.725) and εNd values from -13.7 to -9.4 (Awasthi and Ray, 2020; Chen et al., 2002; Xu et al., 2008). In addition, gneissic rock of the southern Indian continent displays $^{87}Sr/^{86}Sr$ values from 0.702 to 0.719 and unradiogenic εNd values from -41.9 to -26.5 (Peucat et al., 1989).

As shown in Figure 3b, most samples from ODP Site 758 plot in the mixing area

of the Sibumasu block, peninsular gneisses and the G-B river system, suggesting multiple sediment sources. Specifically, we note that most of the sediments at Site 758 that are older than ~22 Ma are a mixture between two end-members: the Sibumasu block and Indian peninsular gneisses. In contrast, the sediments of Site 758 that are younger than 22 Ma seem more likely to have at least three end-members mixing, with the addition of the G-B river system at that time (Fig. 3b). This interpretation is also supported by the exceptionally consistent variation in Sr and Nd isotopic compositions between 22 and 13 Ma (Fig. 2), which contradicts the fact that two end-member mixtures would be expected to show a negative correlation of Sr and Nd isotopic compositions (Faure, 1977). Since approximately 8 Ma, the Site 758 samples clearly shift closer to the Himalayan river system (Fig. 3b) and plot in the field of modern sediments of the eastern part of the Bengal Fan (Colin et al., 1999). This result suggests a strong contribution of sediments from the Irrawaddy and Brahmaputra Rivers.

Moreover, according to the paleogeographic reconstruction and India-Asia plate evolutionary history (Awasthi and Ray, 2020; Kessarkar et al., 2003; Zhang et al., 2017) (Fig. 5a), the Greater Indian continent block was located southwest of the modern Indian continent, and the study site was very close to the southern Indian continent but was far from the South Asian margin in the Eocene-Oligocene (Zhang et al., 2017). Thus, we suggest that gneissic rock of the southern Indian continent and the Sibumasu rocks of the west Burma block might be two major sources for the study site between 37 and 22 Ma. In contrast, with the northwestward movement of the

Indian Peninsula and uplift of the Himalayan orogen (Zhang et al., 2017), the sediment contribution to the study area from the Himalayan river system became more important and dominant after ~22 Ma and 8 Ma, respectively.

Combined with the clay mineral results discussed above, we conclude that the long-term evolution of the sediment source to the study site that has occurred since the late Eocene can be divided into three stages: Stage 1 (37-22 Ma) is characterized by the most smectite-rich sediments and low $^{87}Sr/^{86}Sr$ and unradiogenic εNd values, and the sediments mainly originated from the weathering of gneissic rock of the stable southern Indian continent and Sibumasu rocks of the west Burma block; Stage 2 (22-8 Ma) is characterized by smectite-rich sediments containing more illite/chlorite in addition to high $^{87}Sr/^{86}Sr$ and more radiogenic εNd values and was dominated by terrigenous material eroded from the eastern Himalaya with minor contributions from southern India and the Sibumasu rocks; and Stage 3 (<8 Ma) is characterized by illite-chlorite-rich sediments with the highest $^{87}Sr/^{86}Sr$ and relatively more radiogenic εNd values, indicating that the Irrawaddy and Brahmaputra Rivers became the main sources of the Site 758 after ~8 Ma. The increase in the relative proportion of illite and chlorite implies a higher contribution of clay minerals derived from the physical erosion of high relief. Notably, a provenance study from the Andaman Islands suggests that since the early Miocene, sediment sources from the Indo-Burman Ranges and the Myanmar Arc have become the major contributors to the Andaman Basin through the Irrawaddy River system (Awasthi et al., 2020; Awasthi and Ray, 2020), which is consistent with the major conclusion in this study.

5.4 Controls on the long-term paleoenvironmental evolution in South Asia

The provenance variation at ODP Site 758 possibly suggests a causal link between the evolution of the river system and sedimentary basin with tectonic and climatic events in South Asia since ~37 Ma. Here we test these hypotheses by directly comparing the history and timing of major paleoenvironmental, climatic and tectonic events in South Asia.

Our clay mineral and Sr-Nd isotope evidence strongly indicates that the gradual development of the South Asian river system (Brahmaputra River and Irrawaddy River) between approximately 22-8 Ma and its final establishment by ~8 Ma. This hypothesis is supported by the variation in sediment budget in the BoB (Krishna et al., 2016) and the terrigenous MAR at ODP Site 758 (this study) (Fig. 4d), both of which show a rapidly increasing sediment flux at around ~23 Ma and after 8 Ma. A recent provenance study of IODP Site U1480 also indicates that Himalayan-derived sediments have been transported to the Nicobar Fan since ~22.5 Ma (Fig. 4d), and the Nicobar Fan (near ODP Site 758) deposition began at that time (Pickering et al., 2020). In addition, the MAR of the IODP Site U1480 increased abruptly at ~9 Ma, suggesting that the Nicobar Fan sediment supply has sharply increased since then (Fig. 4d) (Pickering et al., 2020). Besides, a recent sedimentary study in the Andaman Ridge also demonstrated that the Irrawaddy River has been the main source of sediment in the Andaman basin since the early Miocene (Awasthi and Ray, 2020). All these findings strongly suggest the enhanced erosion in Himalayan regions and related

possible drainage reorganization in South Asia during the early-late Miocene.

The development of river systems in Asia is closely linked to the evolving topography and Tibetan Plateau uplift, as crustal deformation created regional elevated terrain that provides potential energy to rivers and glaciers, the main agents of erosion (Clark et al., 2004; Zheng et al., 2013). For example, the Yangtze River was likely established before 23 Ma, which might also have been due to tectonic uplift in eastern Tibet (Zheng et al., 2013). This hypothesis is supported by the most significant deformation and the most intensive metamorphic and magmatic activity that occurred throughout the Greater Himalaya since 23 Ma ago (Fig. 4f) (Clift et al., 2008), Data from the Greater Himalayan Crystalline Series support a 25-23 Ma age for the onset of exhumation (Harris, 2007), and exhumation was quite vigorous during the early Miocene (Hodges, 2006). U-Pb dating of zircons in the Qiabulin suggests that the proto-Himalaya grew rapidly beginning in the early Miocene and achieved at least ~5.5 km by ~15 Ma (Fig. 4g) (Ding et al., 2017). Previous studies have also suggested that the southernmost part of the HTP became close to its present altitude approximately 11-9 Ma ago (Rowley and Currie, 2006; Saylor et al., 2009). Therefore, it seems that the HTP region experienced a two-phase major tectonic uplift at ~22 and 8 Ma (Wang et al., 2012). With the establishment of the South Asian river system driven by tectonic deformation in Himalayan regions, large amounts of fluvial materials were delivered directly into the proto-Bengal Fan and thus the ODP Site 758 since the early Miocene.

In addition to tectonic activity, the influence of climatic factors on the fluvial

flux to the BoB should also be considered. Climatic factors, such as temperature and precipitation, can also influence clay mineral assemblages during weathering and erosion processes (Clift et al., 2014; Wan et al., 2015). For example, kaolinite is formed in soils developed in regions with warm and humid climates and adequate drainage conditions, whereas illite and chlorite are the products of physical erosion from bedrock or are formed by weathering of feldspars and micas under moderate hydrolysis conditions (Chamley, 1989). Mean global $\delta^{18}O$ values after ~14 Ma indicate that the global climate shifted from a middle Miocene climate optimum to a late Cenozoic icehouse, which was characterized by gradual cooling and development of a major ice-sheet in Antarctica after ~13.8 Ma (Fig. 4a) (Flower and Kennett, 1994). Therefore, global cooling after the late Miocene might suppress the chemical weathering intensity (Clift et al., 2014; Wan et al., 2012a) and thus influence clay mineral composition in the source region of the study site. Furthermore, the extension of mountain glaciers with global cooling increased the glacier activity in and physical erosion of highlands, which might have provided more radiogenic εNd values and lower $^{87}Sr/^{86}Sr$ ratios with more illite/chlorite sediments derived from the Indo-Burman Ranges, Myanmar Arc and east Himalaya since ~13.8 Ma.

In addition to temperature, hydrologic conditions are another important factor controlling chemical weathering (White and Blum, 1995). The history of the Indian monsoon is poorly known prior to approximately 14 Ma is poorly known and, since the middle Miocene, it remains highly controversial (Clift and Webb, 2018). C_4 grassland expansion inferred from paleosol carbonate $\delta^{18}O$ and $\delta^{13}O$ data in Pakistan

and Nepal indicates that the strengthening of the Indian monsoon and related drying started at 7-8 Ma (Fig. 4c) (Quade et al., 1989), while monsoonal upwelling in the western Arabian Sea likely started at 7.4 Ma (Fig. 4c) (Kroon et al., 1991), 10-11 Ma (Zhuang et al., 2017) or 12.9 Ma (Gupta et al., 2015). In contrast, researchers have also argued for a weakening monsoon and drying climate at approximately 8 Ma by decreased chemical weathering (Clift et al., 2008; Derry and France-Lanord, 1996) and physical erosion (Burbank et al., 1993). During the late Miocene (7-5.4 Ma), the global climate experienced sustained cooling and transient glaciation in the Northern Hemisphere (Herbert et al., 2016), although global deep-sea $\delta^{18}O$ values remained relatively stable (Fig. 4a) (Zachos et al., 2001). In this case, the dry and cool climate-induced weakened chemical weathering could partly account for the higher contents of illite and chlorite at the study site after approximately 8 Ma, during which the sediment provenance of our study site remained relatively stable based on Sr-Nd isotopes (Fig.2). The Indian monsoon-driven climate might also have caused a rapid change in the relative content of clay minerals since the late Miocene.

Based on the correlation of the major tectonic and climatic events combined with previous studies as discussed above (Clift et al., 2008; Ding et al., 2017; Kroon et al., 1991; Pickering et al., 2020; Quade et al., 1989; Zachos et al., 2001), we propose a schematic map (Fig. 5) to show the long-term evolution of the paleogeography and river system (Brahmaputra and Irrawaddy Rivers) in South Asia since the late Eocene. In summary, we conclude that the provenance variation in clay-sized fraction sediments to ODP Site 758 on the Ninetyeast Ridge at ~22 and 8 Ma was indeed a

sedimentary response to drainage reorganization in South Asia, which was possibly caused by tectonic uplift in the Himalaya and southeastern Tibetan Plateau. In addition, rapid global cooling in the late Miocene might also be a significant factor influencing the physical erosion and chemical weathering in Himalayan river systems, which produced more illite- and chlorite-rich clay mineral assemblages at the study site thereafter.

6. Conclusions

To reveal the long-term evolution of sediment provenance and paleoenvironmental evolution of the BoB in South Asia, we investigated clay mineral and Sr-Nd isotopic compositions of <2 μm silicate sediments at ODP Site 758 in the southern BoB since 37 Ma. Sediment provenance variation at the study site was mostly affected by paleogeographic evolution, tectonic uplift of the HTP and/or global cooling. Meanwhile, the development of the South Asian river system might have started in the early Miocene due to the tectonic uplift of the Himalayan region.

Our results show significant temporal variation in the composition of clay-sized sediment sources at the study site, particularly at ~22 Ma and 8 Ma, which in turn was interpreted as a sedimentary response to drainage reorganization in South Asia. We suggest that the Brahmaputra and Irrawaddy Rivers might have been initiated and fully established in the early and late Miocene, respectively. Global cooling after the late Miocene probably strengthened the physical weathering in South Asia and contributed more illite and chlorite to the BoB.

Acknowledgments

We acknowledge the Ocean Drilling Program and the scientific party and technicians of ODP Expedition 121 for recovering the samples. This work was supported by Strategic Priority Research Program of Chinese Academy of Sciences [XDB40010100], National Natural Science Foundation of China [42076052, 41622603], Taishan and Aoshan Talents program [2017ASTCP-ES01], and Innovation project of Qingdao National Laboratory for Marine Science and Technology [2016ASKJ13 and MGQNLM-TD201805]. The support provided by China Scholarship Council (CSC) during a visit of Zehua Song to Université Paris-Saclay is also acknowledged.

Declaration of Competing Interest

All the authors declare no conflicts of interests.

References

Ahmad, S.M., Anil Babu, G., Padmakumari, V.M., Dayal, A.M., Sukhija, B.S., Nagabhushanam, P., 2005. Sr, Nd isotopic evidence of terrigenous flux variations in the Bay of Bengal: Implications of monsoons during the last ~ 34,000 years. Geophysical Research Letters 32.

Ahmad, S.M., Padmakumari, V.M., Babu, G.A., 2009. Strontium and neodymium isotopic compositions in sediments from Godavari, Krishna and Pennar rivers. Current science 1766–1769.

Ali, S., Hathorne, E.C., Frank, M., Gebregiorgis, D., Stattegger, K., Stumpf, R., Kutterolf, S., Johnson, J.E., Giosan, L., 2015. South Asian monsoon history over the past 60 kyr recorded by radiogenic isotopes and clay mineral assemblages in the Andaman Sea. Geochemistry, Geophysics, Geosystems 16, 505–521.

Amidon, W.H., Hynek, S.A., 2010. Exhumational history of the north central Pamir. Tectonics 29.

An, Z., Kutzbach, J.E., Prell, W.L., Porter, S.C., 2001. Evolution of Asian monsoons and phased uplift of the Himalaya–Tibetan plateau since Late Miocene times. Nature 411, 62. https://doi.org/10.1038/35075035

Awasthi, N., George, B.G., Ray, J.S., 2020. Tracing the Sources and Depositional Pathways for the Oligocene Sediments in the Andaman Forearc, in: The Andaman Islands and Adjoining Offshore: Geology, Tectonics and Palaeoclimate. Springer, pp. 93–106.

Awasthi, N., Ray, E., Paul, D., 2018. Sr and Nd isotope compositions of alluvial sediments from the Ganga Basin and their use as potential proxies for source identification and apportionment. Chemical Geology 476, 327–339. https://doi.org/10.1016/j.chemgeo.2017.11.029

Awasthi, N., Ray, J.S., 2020. The Palaeogene record of Himalayan erosion in the

Andaman Basin. Journal of Earth System Science 129, 1–16.

Awasthi, N., Ray, J.S., Singh, A.K., Band, S.T., Rai, V.K., 2014. Provenance of the L ate Quaternary sediments in the Andaman Sea: Implications for monsoon variability and ocean circulation. Geochemistry, Geophysics, Geosystems 15, 3890–3906.

Banerjee, B., Ahmad, S.M., Raza, W., Raza, T., 2017. Paleoceanographic changes in the Northeast Indian Ocean during middle Miocene inferred from carbon and oxygen isotopes of foraminiferal fossil shells. Palaeogeography, Palaeoclimatology, Palaeoecology 466, 166–173.

Barley, M.E., Pickard, A.L., Zaw, K., Rak, P., Doyle, M.G., 2003. Jurassic to Miocene magmatism and metamorphism in the Mogok metamorphic belt and the India-Eurasia collision in Myanmar. Tectonics 22. https://doi.org/10.1029/2002TC001398

Bhattacharya, S., Pande, K., Kumar, A., Kingson, O., Ray, J.S., 2020. Timing of Formation and Obduction of the Andaman Ophiolite, in: The Andaman Islands and Adjoining Offshore: Geology, Tectonics and Palaeoclimate. Springer, pp. 19–42.

Biscaye, P.E., 1965. Mineralogy and sedimentation of recent deep-sea clay in the Atlantic Ocean and adjacent seas and oceans. Geological Society of America Bulletin 76, 803–832.

Burbank, D.W., Derry, L.A., France-Lanord, C., 1993. Reduced Himalayan sediment production 8 Myr ago despite an intensified monsoon. Nature 364, 48–50.

Cao, L., Shao, L., Qiao, P., Zhao, Z., van Hinsbergen, D.J., 2018. Early Miocene birth of modern Pearl River recorded low-relief, high-elevation surface formation of SE Tibetan Plateau. Earth Planetary Science Letters 496, 120–131.

Chamley, H., 1989. Clay sedimentology. Springer Science & Business Media.

Chen, F., Satir, M., Ji, J., Zhong, D., 2002. Nd–Sr–Pb isotopes of Tengchong Cenozoic volcanic rocks from western Yunnan, China: evidence for an enriched-mantle source. Journal of Asian Earth Sciences 21, 39–45.

Chen, J., Li, G., Yang, J., Rao, W., Lu, H., Balsam, W., Sun, Y., Ji, J., 2007. Nd and Sr isotopic characteristics of Chinese deserts: implications for the provenances of Asian dust. Geochimica et Cosmochimica Acta 71, 3904–3914.

Clark, M.K., Schoenbohm, L.M., Royden, L.H., Whipple, K.X., Burchfiel, B.C., Zhang, X., Tang, W., Wang, E., Chen, L., 2004. Surface uplift, tectonics, and erosion of eastern Tibet from large-scale drainage patterns. Tectonics 23.

Clift, P.D., Blusztajn, J., Nguyen, A.D., 2006. Large-scale drainage capture and surface uplift in eastern Tibet–SW China before 24 Ma inferred from sediments of the Hanoi Basin, Vietnam. Geophysical Research Letters 33.

Clift, P.D., Hodges, K.V., Heslop, D., Hannigan, R., Van Long, H., Calves, G., 2008. Correlation of Himalayan exhumation rates and Asian monsoon intensity. Nature geoscience 1, 875.

Clift, P.D., Kulhanek, D.K., Zhou, P., Bowen, M.G., Vincent, S.M., Lyle, M., Hahn, A., 2020. Chemical weathering and erosion responses to changing monsoon climate in the Late Miocene of Southwest Asia. Geological Magazine 157,

939–955.

Clift, P.D., Wan, S., Blusztajn, J., 2014. Reconstructing chemical weathering, physical erosion and monsoon intensity since 25 Ma in the northern South China Sea: a review of competing proxies. Earth-Science Reviews 130, 86–102.

Clift, P.D., Webb, A.A.G., 2018. A history of the Asian monsoon and its interactions with solid Earth tectonics in Cenozoic South Asia. Geological Society, London, Special Publications 483, 631–652.

Colin, C., Turpin, L., Bertaux, J., Desprairies, A., Kissel, C., 1999. Erosional history of the Himalayan and Burman ranges during the last two glacial–interglacial cycles. Earth Planetary Science Letters 171, 647–660.

Colin, C., Turpin, L., Blamart, D., Frank, N., Kissel, C., Duchamp, S., 2006. Evolution of weathering patterns in the Indo-Burman Ranges over the last 280 kyr: Effects of sediment provenance on 87Sr/86Sr ratios tracer. Geochemistry, Geophysics, Geosystems 7.

Curray, J.R., 2014. The Bengal depositional system: from rift to orogeny. Marine Geology 352, 59–69.

Curray, J.R., Emmel, F.J., Moore, D.G., 2002. The Bengal Fan: morphology, geometry, stratigraphy, history and processes. Marine Petroleum Geology 19, 1191–1223.

Dai, J., Zhao, X., Wang, C., Zhu, L., Li, Y., Finn, D., 2012. The vast proto-Tibetan plateau: New constraints from paleogene Hoh Xil basin. Gondwana Research 22, 434–446.

Damodararao, K., Singh, S.K., Rai, V.K., Ramaswamy, V., Rao, P.S., 2016. Lithology, monsoon and sea-surface current control on provenance, dispersal and deposition of sediments over the Andaman continental shelf. Frontiers in Marine Science 3, 118.

Deeken, A., Thiede, R.C., Sobel, E.R., Hourigan, J.K., Strecker, M.R., 2011. Exhumational variability within the Himalaya of northwest India. Earth Planetary Science Letters 305, 103–114.

Derry, L.A., France-Lanord, C., 1996. Neogene Himalayan weathering history and river87Sr86Sr: impact on the marine Sr record. Earth Planetary Science Letters 142, 59–74.

Ding, L., Spicer, R.A., Yang, J., Xu, Q., Cai, F., Li, S., Lai, Q., Wang, H., Spicer, T.E.V., Yue, Y., 2017. Quantifying the rise of the Himalaya orogen and implications for the South Asian monsoon. Geology 45, 215–218.

Fagel, N., 2007. Chapter Four Clay Minerals, Deep Circulation and Climate, in: Hillaire–Marcel, C., De Vernal, A. (Eds.), Developments in Marine Geology, Proxies in Late Cenozoic Paleoceanography. Elsevier, pp. 139–184. https://doi.org/10.1016/S1572-5480(07)01009-3

Farrell, J.W., Janecek, T.R., 1991. Late Neogene paleoceanography and paleoclimatology of the northeast Indian Ocean (Site 758). Presented at the Weissel, J., Peirce, J., Taylor, E., Alt, J., et al., Proc. ODP, Sci. Results, pp. 297–355.

Faure, G., 1977. Principles of isotope geology.

Flower, B.P., Kennett, J.P., 1994. The middle Miocene climatic transition: East Antarctic ice sheet development, deep ocean circulation and global carbon cycling. Palaeogeography, Palaeoclimatology, Palaeoecology 108, 537–555.

France-Lanord, C., Derry, L., Michard, A., 1993. Evolution of the Himalaya since Miocene time: isotopic and sedimentological evidence from the Bengal Fan. Geological Society, London, Special Publications 74, 603–621.

France-Lanord, C., Derry, L.A., 1997. Organic carbon burial forcing of the carbon cycle from Himalayan erosion. Nature 390, 65–67.

France-Lanord, C., Schwenk, T., Klaus, A., 2014. Bengal Fan: Neogene and late Paleogene record of Himalayan orogeny and climate: a transect across the Middle Bengal Fan. International Ocean Discovery Program Scientific Prospectus 354.

Galy, V., France-Lanord, C., Peucker-Ehrenbrink, B., Huyghe, P., 2010. Sr–Nd–Os evidence for a stable erosion regime in the Himalaya during the past 12 Myr. Earth Planetary Science Letters 290, 474–480.

George, A.D., Marshallsea, S.J., Wyrwoll, K.-H., Jie, C., Yanchou, L., 2001. Miocene cooling in the northern Qilian Shan, northeastern margin of the Tibetan Plateau, revealed by apatite fission-track and vitrinite-reflectance analysis. Geology 29, 939–942.

Gourlan, A.T., Meynadier, L., Allègre, C.J., 2008. Tectonically driven changes in the Indian Ocean circulation over the last 25 Ma: Neodymium isotope evidence. Earth and Planetary Science Letters 267, 353–364.

https://doi.org/10.1016/j.epsl.2007.11.054

Guo, Z.T., Sun, B., Zhang, Z.S., Peng, S.Z., Xiao, G.Q., Ge, J.Y., Hao, Q.Z., Qiao, Y.S., Liang, M.Y., Liu, J.F., Yin, Q.Z., Wei, J.J., 2008. A major reorganization of Asian climate regime by the early Miocene. Climate of the Past Discussions 4, 535–584.

Gupta, A.K., Yuvaraja, A., Prakasam, M., Clemens, S.C., Velu, A., 2015. Evolution of the South Asian monsoon wind system since the late Middle Miocene. Palaeogeography, Palaeoclimatology, Palaeoecology 438, 160–167.

Harris, N., 2007. Channel flow and the Himalayan–Tibetan orogen: a critical review. Journal of the Geological Society 164, 511–523.

Harris, N., 2006. The elevation history of the Tibetan Plateau and its implications for the Asian monsoon. Palaeogeography, Palaeoclimatology, Palaeoecology 241, 4–15.

Herbert, T.D., Lawrence, K.T., Tzanova, A., Peterson, L.C., Caballero-Gill, R., Kelly, C.S., 2016. Late Miocene global cooling and the rise of modern ecosystems. Nature Geoscience 9, 843–847.

Heroy, D.C., Kuehl, S.A., Goodbred, S.L., 2003. Mineralogy of the Ganges and Brahmaputra Rivers: implications for river switching and Late Quaternary climate change. Sedimentary Geology, Sedimentary Geology of the Bengal Basin, Bangladesh, in relation to the Asia-Greater India collision and the evolution of the eastern Bay of Bengal 155, 343–359. https://doi.org/10.1016/S0037-0738(02)00186-0

Hoang, L. van, Wu, F.-Y., Clift, P.D., Wysocka, A., Swierczewska, A., 2009. Evaluating the evolution of the Red River system based on in situ U-Pb dating and Hf isotope analysis of zircons. Geochemistry, Geophysics, Geosystems 10. https://doi.org/10.1029/2009GC002819

Hodges, K., 2006. Climate and the evolution of mountains. Scientific American 295, 72–79.

Hoke, G.D., Liu-Zeng, J., Hren, M.T., Wissink, G.K., Garzione, C.N., 2014. Stable isotopes reveal high southeast Tibetan Plateau margin since the Paleogene. Earth Planetary Science Letters 394, 270–278.

Hough, B.G., Garzione, C.N., Wang, Z., Lease, R.O., Burbank, D.W., Yuan, D., 2011. Stable isotope evidence for topographic growth and basin segmentation: Implications for the evolution of the NE Tibetan Plateau. Bulletin 123, 168–185.

Hu, X., Garzanti, E., Wang, J., Huang, W., An, W., Webb, A., 2016. The timing of India-Asia collision onset–Facts, theories, controversies. Earth-Science Reviews 160, 264–299.

Huizing, H.G.J., 1971. A reconnaissance study of the mineralogy of sand fractions from East Pakistan sediments and soils. Geoderma 6, 109–133. https://doi.org/10.1016/0016-7061(71)90029-2

Huyghe, P., Guilbaud, R., Bernet, M., Galy, A., Gajurel, A.P., 2011. Significance of the clay mineral distribution in fluvial sediments of the Neogene to Recent Himalayan Foreland Basin (west-central Nepal). Basin Research 23, 332–345.

Joussain, R., Colin, C., Liu, Z., Meynadier, L., Fournier, L., Fauquembergue, K., Zaragosi, S., Schmidt, F., Rojas, V., Bassinot, F., 2016. Climatic control of sediment transport from the Himalayas to the proximal NE Bengal Fan during the last glacial-interglacial cycle. Quaternary Science Reviews 148, 1–16. https://doi.org/10.1016/j.quascirev.2016.06.016

Kessarkar, P.M., Rao, V.P., Ahmad, S.M., Babu, G.A., 2003. Clay minerals and Sr–Nd isotopes of the sediments along the western margin of India and their implication for sediment provenance. Marine Geology 202, 55–69.

Khan, M.H.R., Liu, J., Liu, S., Seddique, A.A., Cao, L., Rahman, A., 2019. Clay mineral compositions in surface sediments of the Ganges-Brahmaputra-Meghna river system of Bengal Basin, Bangladesh. Marine Geology 412, 27–36.

Kolla, V., Moore, D.G., Curray, J.R., 1976. Recent bottom-current activity in the deep western Bay of Bengal. Marine Geology 21, 255–270.

Krishna, K.S., Ismaiel, M., Srinivas, K., Rao, D.G., Mishra, J., Saha, D., 2016. Sediment pathways and emergence of Himalayan source material in the Bay of Bengal. Current Science 363–372.

Kroon, D., Steens, T., Troelstra, S.R., 1991. Onset of Monsoonal related upwelling in the western Arabian Sea as revealed by planktonic foraminifers. Proceedings of the Ocean Drilling Program, Scientific Results 257–263.

Lease, R.O., Burbank, D.W., Clark, M.K., Farley, K.A., Zheng, D., Zhang, H., 2011. Middle Miocene reorganization of deformation along the northeastern Tibetan

Plateau. Geology 39, 359–362.

Lee, J., Kim, S., Lee, J.I., Cho, H.G., Phillips, S.C., Khim, B.-K., 2020. Monsoon-influenced variation of clay mineral compositions and detrital Nd-Sr isotopes in the western Andaman Sea (IODP Site U1447) since the late Miocene. Palaeogeography, Palaeoclimatology, Palaeoecology 538, 109339.

Lenard, S.J.P., Lavé, J., France-Lanord, C., Aumaître, G., Bourlès, D.L., Keddadouche, K., 2020. Steady erosion rates in the Himalayas through late Cenozoic climatic changes. Nature Geoscience 13, 448–452. https://doi.org/10.1038/s41561-020-0585-2

Li, J., Liu, S., Shi, X., Feng, X., Fang, X., Cao, P., Sun, X., Wenxing, Y., Khokiattiwong, S., Kornkanitnan, N., 2017. Distributions of clay minerals in surface sediments of the middle Bay of Bengal: Source and transport pattern. Continental Shelf Research 145, 59–67. https://doi.org/10.1016/j.csr.2017.06.017

Licht, A., France-Lanord, C., Reisberg, L., Fontaine, C., Soe, A.N., Jaeger, J.-J., 2013. A palaeo Tibet–Myanmar connection? Reconstructing the Late Eocene drainage system of central Myanmar using a multi-proxy approach. Journal of the Geological Society 2012–126.

Licht, A., Reisberg, L., France-Lanord, C., Soe, A.N., Jaeger, J.-J., 2016. Cenozoic evolution of the central Myanmar drainage system: insights from sediment provenance in the Minbu Sub-Basin. Basin Research 28, 237–251.

Licht, A., Van Cappelle, M., Abels, H.A., Ladant, J.-B., Trabucho-Alexandre, J.,

France-Lanord, C., Donnadieu, Y., Vandenberghe, J., Rigaudier, T., Lécuyer, C., 2014. Asian monsoons in a late Eocene greenhouse world. Nature 513, 501–506.

Lightfoot, P., Hawkesworth, C., 1988. Origin of Deccan Trap lavas: evidence from combined trace element and Sr-, Nd-and Pb-isotope studies. Earth Planetary Science Letters 91, 89–104.

Lin, T.-H., Lo, C.-H., Chung, S.-L., Hsu, F.-J., Yeh, M.-W., Lee, T.-Y., Ji, J.-Q., Wang, Y.-Z., Liu, D., 2009. 40Ar/39Ar dating of the Jiali and Gaoligong shear zones: Implications for crustal deformation around the Eastern Himalayan Syntaxis. Journal of Asian Earth Sciences 34, 674–685. https://doi.org/10.1016/j.jseaes.2008.10.009

Lupker, M., France-Lanord, C., Galy, V., Lavé, J., Kudrass, H., 2013. Increasing chemical weathering in the Himalayan system since the Last Glacial Maximum. Earth Planetary Science Letters 365, 243–252.

McNeill, L.C., Dugan, B., Backman, J., Pickering, K.T., Pouderoux, H.F., Henstock, T.J., Petronotis, K.E., Carter, A., Chemale Jr, F., Milliken, K.L., 2017. Understanding Himalayan erosion and the significance of the Nicobar Fan. Earth Planetary Science Letters 475, 134–142.

Meyer, I., Davies, G.R., Stuut, J.-B.W., 2011. Grain size control on Sr-Nd isotope provenance studies and impact on paleoclimate reconstructions: An example from deep-sea sediments offshore NW Africa. Geochemistry, Geophysics, Geosystems 12.

Milliman, J.D., Farnsworth, K.L., 2011. River discharge to the coastal ocean.

Misra, S., Froelich, P.N., 2012. Lithium isotope history of Cenozoic seawater: changes in silicate weathering and reverse weathering. Science 335, 818–823.

Mitchell, A., Chung, S.-L., Oo, T., Lin, T.-H., Hung, C.-H., 2012. Zircon U–Pb ages in Myanmar: Magmatic–metamorphic events and the closure of a neo-Tethys ocean? Journal of Asian Earth Sciences 56, 1–23.

Mitchell, A.H.G., Htay, M.T., Htun, K.M., Win, M.N., Oo, T., Hlaing, T., 2007. Rock relationships in the Mogok metamorphic belt, Tatkon to Mandalay, central Myanmar. Journal of Asian Earth Sciences 29, 891–910. https://doi.org/10.1016/j.jseaes.2006.05.009

Mokadem, F., Parkinson, I.J., Hathorne, E.C., Anand, P., Allen, J.T., Burton, K.W., 2015. High-precision radiogenic strontium isotope measurements of the modern and glacial ocean: Limits on glacial–interglacial variations in continental weathering. Earth and Planetary Science Letters 415, 111–120.

Molnar, P., England, P., 1990. Late Cenozoic uplift of mountain ranges and global climate change: chicken or egg? Nature 346, 29–34.

Molnar, P., England, P., Martinod, J., 1993. Mantle dynamics, uplift of the Tibetan Plateau, and the Indian monsoon. Reviews of Geophysics 31, 357–396.

Nesbitt, H.W., Grant M. Young, 1996. Petrogenesis of sediments in the absence of chemical weathering: effects of abrasion and sorting on bulk composition and mineralogy. Sedimentology 43, 341–358.

Peucat, J.J., Vidal, P., Bernard-Griffiths, J., Condie, K.C., 1989. Sr, Nd, and Pb

isotopic systematics in the Archean low-to high-grade transition zone of southern India: syn-accretion vs. post-accretion granulites. The Journal of Geology 97, 537–549.

Phillips, S.C., Johnson, J.E., Underwood, M.B., Guo, J., Giosan, L., Rose, K., 2014. Long-timescale variation in bulk and clay mineral composition of Indian continental margin sediments in the Bay of Bengal, Arabian Sea, and Andaman Sea. Marine Petroleum Geology 58, 117–138.

Pickering, K.T., Pouderoux, H., McNeill, L.C., Backman, J., Chemale, F., Kutterolf, S., Milliken, K.L., Hideki, M., Henstock, T.J., Stevens, D.E., 2020. Sedimentology, stratigraphy and architecture of the Nicobar Fan (Bengal–Nicobar Fan System), Indian Ocean: Results from International Ocean Discovery Program Expedition 362. Sedimentology.

Pierce, J., Weissel, J., Taylat, E., 1989. Proceeding Ocean Drilling Program. Init. Repts., 121, Ocean Drilling Porgram.

Polissar, P.J., Freeman, K.H., Rowley, D.B., McInerney, F.A., Currie, B.S., 2009. Paleoaltimetry of the Tibetan Plateau from D/H ratios of lipid biomarkers. Earth Planetary Science Letters 287, 64–76.

Prell, W.L., Kutzbach, J.E., 1992. Sensitivity of the Indian monsoon to forcing parameters and implications for its evolution. Nature 360, 647.

Quade, J., Cerling, T.E., Bowman, J.R., 1989. Development of Asian monsoon revealed by marked ecological shift during the latest Miocene in northern Pakistan. Nature 342, 163–166.

Rao, V.P., Kessarkar, P.M., 2001. Geomorphology and geology of the Bay of Bengal and the Andaman Sea.

Raymo, M.E., Ruddiman, W., 1992. Tectonic forcing of late Cenozoic climate. Nature 359, 117–122.

Rea, D.K., Janecek, T.R., 1981. Late cretaceous history of eolian deposition in the mid-pacific mountains, central North Pacific Ocean.

Révillon, S., Jouet, G., Bayon, G., Rabineau, M., Dennielou, B., Hémond, C., Berné, S., 2011. The provenance of sediments in the Gulf of Lions, western Mediterranean Sea. Geochemistry, Geophysics, Geosystems 12.

Robinson, R.A.J., Brezina, C.A., Parrish, R.R., Horstwood, M.S.A., Nay Win, O., Bird, M.I., Myint, T., Walters, A.S., Oliver, G.J.H., Khin, Z., 2014. Large rivers and orogens: The evolution of the Yarlung Tsangpo–Irrawaddy system and the eastern Himalayan syntaxis. Gondwana Research 26, 112–121. https://doi.org/10.1016/j.gr.2013.07.002

Rodolfo, K.S., 1969. Sediments of the Andaman basin, northeastern Indian Ocean. Marine Geology 7, 371–402.

Rowley, D.B., Currie, B.S., 2006. Palaeo-altimetry of the late Eocene to Miocene Lunpola basin, central Tibet. Nature 439, 677.

Sarin, M.M., Krishnaswami, S., Dilli, K., Somayajulu, B.L.K., Moore, W.S., 1989. Major ion chemistry of the Ganga-Brahmaputra river system: Weathering processes and fluxes to the Bay of Bengal. Geochimica et cosmochimica acta 53, 997–1009.

Saylor, J.E., Quade, J., Dettman, D.L., DeCelles, P.G., Kapp, P.A., Ding, L., 2009. The late Miocene through present paleoelevation history of southwestern Tibet. American Journal of Science 309, 1–42.

Shankar, D., Vinayachandran, P.N., Unnikrishnan, A.S., 2002. The monsoon currents in the north Indian Ocean. Progress in Oceanography 52, 63–120. https://doi.org/10.1016/S0079-6611(02)00024-1

Shen, X., Wan, S., France-Lanord, C., Clift, P.D., Tada, R., Révillon, S., Shi, X., Zhao, D., Liu, Y., Yin, X., Song, Z., Li, A., 2017. History of Asian eolian input to the Sea of Japan since 15 Ma: Links to Tibetan uplift or global cooling? Earth and Planetary Science Letters 474, 296–308. https://doi.org/10.1016/j.epsl.2017.06.053

Sijinkumar, A.V., Clemens, S., Nath, B.N., Prell, W., Benshila, R., Lengaigne, M., 2016. δ18O and salinity variability from the Last Glacial Maximum to Recent in the Bay of Bengal and Andaman Sea. Quaternary Science Reviews 135, 79–91. https://doi.org/10.1016/j.quascirev.2016.01.022

Singh, S.K., France-Lanord, C., 2002. Tracing the distribution of erosion in the Brahmaputra watershed from isotopic compositions of stream sediments. Earth Planetary Science Letters 202, 645–662.

Singh, S.K., Rai, S.K., Krishnaswami, S., 2008. Sr and Nd isotopes in river sediments from the Ganga Basin: sediment provenance and spatial variability in physical erosion. Journal of Geophysical Research: Earth Surface 113.

Sobel, E.R., Dumitru, T.A., 1997. Thrusting and exhumation around the margins of

the western Tarim basin during the India-Asia collision. Journal of Geophysical Research: Solid Earth 102, 5043–5063.

Stephenson, D., Marshall, T.R., 1984. The petrology and mineralogy of Mt. Popa Volcano and the nature of the late-Cenozoic Burma Volcanic Arc. Journal of the Geological Society 141, 747–762. https://doi.org/10.1144/gsjgs.141.4.0747

Sun, X., Wang, P., 2005. How old is the Asian monsoon system?—Palaeobotanical records from China. Palaeogeography, Palaeoclimatology, Palaeoecology 222, 181–222.

Tada, R., Hongbo Zheng, Peter D. Clift, 2016. Evolution and variability of the Asian monsoon and its potential linkage with uplift of the Himalaya and Tibetan Plateau. Progress in Earth and Planetary Science 3.

Tapponnier, P., Zhiqin, X., Roger, F., Meyer, B., Arnaud, N., Wittlinger, G., Jingsui, Y., 2001. Oblique stepwise rise and growth of the Tibet Plateau. science 294, 1671–1677.

Tripathy, G.R., Singh, S.K., Ramaswamy, V., 2014. Major and trace element geochemistry of Bay of Bengal sediments: Implications to provenances and their controlling factors. Palaeogeography, palaeoclimatology, palaeoecology 397, 20–30.

Wan, S., Clift, P.D., Li, A., Yu, Z., Li, T., Hu, D., 2012a. Tectonic and climatic controls on long-term silicate weathering in Asia since 5 Ma. Geophysical Research Letters 39.

Wan, S., Clift, P.D., Zhao, D., Hovius, N., Munhoven, G., France-Lanord, C., Wang,

Y., Xiong, Z., Huang, J., Yu, Z., Zhang, J., Ma, W., Zhang, G., Li, A., Li, T., 2017. Enhanced silicate weathering of tropical shelf sediments exposed during glacial lowstands: A sink for atmospheric CO2. Geochimica et Cosmochimica Acta 200, 123–144. https://doi.org/10.1016/j.gca.2016.12.010

Wan, S., Li, A., Clift, P.D., Stuut, J.-B.W., 2007. Development of the East Asian monsoon: mineralogical and sedimentologic records in the northern South China Sea since 20 Ma. Palaeogeography, Palaeoclimatology, Palaeoecology 254, 561–582.

Wan, S., Toucanne, S., Clift, P.D., Zhao, D., Bayon, G., Yu, Z., Cai, G., Yin, X., Révillon, S., Wang, D., 2015. Human impact overwhelms long-term climate control of weathering and erosion in southwest China. Geology 43, 439–442.

Wan, S., Yu, Z., Clift, P.D., Sun, H., Li, A., Li, T., 2012b. History of Asian eolian input to the West Philippine Sea over the last one million years. Palaeogeography, Palaeoclimatology, Palaeoecology 326, 152–159.

Wang, C., Dai, J., Zhao, X., Li, Y., Graham, S.A., He, D., Ran, B., Meng, J., 2014. Outward-growth of the Tibetan Plateau during the Cenozoic: A review. Tectonophysics 621, 1–43.

Wang, E., Kirby, E., Furlong, K.P., Van Soest, M., Xu, G., Shi, X., Kamp, P.J., Hodges, K.V., 2012. Two-phase growth of high topography in eastern Tibet during the Cenozoic. Nature Geoscience 5, 640–645.

Wang, P., 2004. Cenozoic deformation and the history of sea-land interactions in Asia. Geophysical Monograph Series 149, 1–22.

Wang, Y., Cheng, H., Edwards, R.L., Kong, X., Shao, X., Chen, S., Wu, J., Jiang, X., Wang, X., An, Z., 2008. Millennial-and orbital-scale changes in the East Asian monsoon over the past 224,000 years. Nature 451, 1090–1093.

White, A.F., Blum, A.E., 1995. Effects of climate on chemical_ weathering in watersheds. Geochimica et Cosmochimica Acta 29, 1729–1747.

Willenbring, J.K., von Blanckenburg, F., 2010. Long-term stability of global erosion rates and weathering during late-Cenozoic cooling. Nature 465, 211–214. https://doi.org/10.1038/nature09044

Xiao, G., Guo, Z., Dupont-Nivet, G., Lu, H., Wu, N., Ge, J., Hao, Q., Peng, S., Li, F., Abels, H.A., 2012. Evidence for northeastern Tibetan Plateau uplift between 25 and 20 Ma in the sedimentary archive of the Xining Basin, Northwestern China. Earth Planetary Science Letters 317, 185–195.

Xu, Y.-G., Lan, J.-B., Yang, Q.-J., Huang, X.-L., Qiu, H.-N., 2008. Eocene break-off of the Neo-Tethyan slab as inferred from intraplate-type mafic dykes in the Gaoligong orogenic belt, eastern Tibet. Chemical Geology 255, 439–453.

Yu, Z., Colin, C., Bassinot, F., Wan, S., Bayon, G., 2020. Climate-driven weathering shifts between highlands and floodplains. Geochemistry, Geophysics, Geosystems e2020GC008936.

Yu, Z., Colin, C., Wan, S., Saraswat, R., Song, L., Xu, Z., Clift, P., Lu, H., Lyle, M., Kulhanek, D., 2019. Sea level-controlled sediment transport to the eastern Arabian Sea over the past 600 kyr: Clay minerals and SrNd isotopic evidence from IODP site U1457. Quaternary Science Reviews 205, 22–34.

Yuan, D.-Y., Ge, W.-P., Chen, Z.-W., Li, C.-Y., Wang, Z.-C., Zhang, H.-P., Zhang, P.-Z., Zheng, D.-W., Zheng, W.-J., Craddock, W.H., 2013. The growth of northeastern Tibet and its relevance to large-scale continental geodynamics: A review of recent studies. Tectonics 32, 1358–1370.

Zachos, J., Pagani, M., Sloan, L., Thomas, E., Billups, K., 2001. Trends, rhythms, and aberrations in global climate 65 Ma to present. science 292, 686–693.

Zhang, J., Wan, S., Clift, P.D., Huang, J., Yu, Z., Zhang, K., Mei, X., Liu, J., Han, Z., Nan, Q., 2019. History of Yellow River and Yangtze River delivering sediment to the Yellow Sea since 3.5 Ma: Tectonic or climate forcing? Quaternary Science Reviews 216, 74–88.

Zhang, P., Mei, L., Xiong, P., Hu, X., Li, R., Qiu, H., 2017. Structural features and proto-type basin reconstructions of the Bay of Bengal Basin: A remnant ocean basin model. Journal of Earth Science 28, 666–682.

Zhang, P., Najman, Y., Mei, L., Millar, I., Sobel, E.R., Carter, A., Barfod, D., Dhuime, B., Garzanti, E., Govin, G., 2019. Palaeodrainage evolution of the large rivers of East Asia, and Himalayan-Tibet tectonics. Earth-Science Reviews 192, 601–630.

Zhang, R., Murphy, M.A., Lapen, T.J., Sanchez, V., Heizler, M., 2011. Late Eocene crustal thickening followed by Early-Late Oligocene extension along the India-Asia suture zone: Evidence for cyclicity in the Himalayan orogen. Geosphere 7, 1249–1268.

Zhang, Z., 2002. Sedimentary records and paleoclimate evolution of Bay of Bengal

since Pliocene time (in Chinese)[dissertation]. Beijing: China University of Geosciences.

Zhao, D., Wan, S., Toucanne, S., Clift, P.D., Tada, R., Révillon, S., Kubota, Y., Zheng, X., Yu, Z., Huang, J., Jiang, H., Xu, Z., Shi, X., Li, A., 2017. Distinct control mechanism of fine-grained sediments from Yellow River and Kyushu supply in the northern Okinawa Trough since the last glacial. Geochemistry, Geophysics, Geosystems 18, 2949–2969. https://doi.org/10.1002/2016gc006764

Zheng, H., Clift, P.D., He, M., Bian, Z., Liu, G., Liu, X., Xia, L., Yang, Q., Jourdan, F., 2020. Formation of the First Bend in the late Eocene gave birth to the modern Yangtze River, China. Geology 49, 35–39. https://doi.org/10.1130/G48149.1

Zheng, H., Clift, P.D., Wang, P., Tada, R., Jia, J., He, M., Jourdan, F., 2013. Pre-miocene birth of the Yangtze River. Proceedings of the National Academy of Sciences 110, 7556–7561.

Zhuang, G., Pagani, M., Zhang, Y.G., 2017. Monsoonal upwelling in the western Arabian Sea since the middle Miocene. Geology 45, 655–658.

Figure Captions

Figure 1. Locations of geographic features, terrestrial and marine records. (a) Location of ODP Site 758 in the southern BoB (red star), and the average isotopic composition of the main formations/rivers ($^{87}Sr/^{86}Sr$ and εNd) are also indicated (Ahmad et al., 2009; Awasthi et al., 2020, 2014; Awasthi and Ray, 2020; Chen et al.,

2002; Colin et al., 1999; Damodararao et al., 2016; Licht et al., 2013; Lightfoot and Hawkesworth, 1988; Peucat et al., 1989; Singh et al., 2008; Singh and France-Lanord, 2002; Xu et al., 2008). The major river systems in the South Asia are also shown by light blue solid lines. The regional circulation pattern influenced by the Indian monsoon with seasonal wind and surface current in the summer is shown by red arrows and in the winter is shown by black arrows (Kolla et al., 1976; Shankar et al., 2002). (b) Locations of sediment cores SK-157-14 (Ahmad et al., 2005), IODP Site U1447 (Lee et al., 2020), IODP Site U1480 (Pickering et al., 2020), DSDP Site 218 (Galy et al., 2010) and ODP Leg Site 717/718 (France-Lanord et al., 1993) in the southern BoB mentioned in this paper are shown by yellow solid circles.

Figure 2. Comparison of the terrigenous mass accumulation rate (MAR), clay mineral assemblages, illite chemical index, crystallinity index, smectite crystallinity index, εNd, and $^{87}Sr/^{86}Sr$ at ODP Site 758 since 37 Ma. The horizontal dashed black line across all frames at approximately 178 and 100 m indicates the boundary of provenance transition at ODP Site 758. Also shown the age control points based on biostratigraphy of calcareous nannofossils (red nail) and diatoms (yellow nail) (Pierce et al., 1989).

Figure 3. Provenance discrimination plot of clay minerals and Sr-Nd isotopes. (a) Smectite-(illite+chlorite)-kaolinite ternary diagram, showing the clay mineral composition of sediments from ODP Site 758 and their potential sources, including

different parts of the modern Ganges-Brahmaputra river system (samples from the upper and lower Ganges and Brahmaputra Rivers) (Khan et al., 2019; Sarin et al., 1989), the modern Irrawaddy River (Rodolfo, 1969), the modern Godavari-Krishna Rivers (Phillips et al., 2014) and sediments from rivers that drain from the Indian peninsular gneissic rocks (Kessarkar et al., 2003) and Andaman-Nicobar Ridge (Ali et al., 2015). (b) Variations in εNd versus $^{87}Sr/^{86}Sr$ at ODP Site 758 and river sediments and bulk rock samples around the BoB. In this diagram, we grouped Sr-Nd isotope data of sediments from the modern Ganges-Brahmaputra Rivers (Singh et al., 2008; Singh and France-Lanord, 2002), the modern Irrawaddy River end-member (Colin et al., 1999; Damodararao et al., 2016), the modern East India Rivers (Godavari-Krishna Rivers) and formations from the Sibumasu block (Awasthi and Ray, 2020; Chen et al., 2002; Xu et al., 2008) and Indian Peninsular gneisses (Peucat et al., 1989).

Figure 4. Marine and terrestrial records since 37 Ma showing the evolution of the paleoenvironment in South Asia, the global climate and major uplift events in the Himalayas. Comparison of the (a) Global deep-sea $\delta^{18}O$ based on data compiled from more than 40 DSDP and ODP sites (Zachos et al., 2001). (b) Clay mineral assemblages at ODP Site 758 (this study). (c) Abundance of *G.bulloides* at ODP Site 730 on the Oman margin as a proxy for the summer monsoon wind strength (Gupta et al., 2015), and the carbon isotope character of pedogenic carbonate in Pakistan as an indicator of dominant vegetation in the Potwar Plateau of Pakistan (Quade et al., 1989). (d) Terrigenous mass accumulation rates ($g/cm^2/ky$) at ODP Site 758 on the

Ninetyeast Ridge (this study) and total mass accumulation rates (g/cm^2/ky) at IODP Site U1480 in the Nicobar Fan (Pickering et al., 2020). (e) εNd values and smectite/(chlorite+illite) ratios at ODP Site 758 in the southern BoB (this study). (f) Exhumation rates of the Greater Himalaya tracked by probability densities for ^{40}Ar/^{39}Ar muscovite dates from the Himalayan hinterland and proximal foreland (Clift et al., 2008). (e) Time-altitude plot for the Himalayan orogen based on Climate Leaf Analysis Multivariate Program (CLAMP) analysis and isotopes; elevations are for basin floors and uncertainties are 2σ (Ding et al., 2017).

Figure 5. Time scales of tectonic schematic diagrams illustrating the reconstructions of the BoB and surrounding areas; (a) late Eocene (~37 Ma), (b) early Miocene (~22 Ma), (c) late Miocene (~8 Ma), and (d) At present. The reconstruction maps are modified from (Awasthi and Ray, 2020; Kessarkar et al., 2003; Zhang et al., 2017).

Table Captions

Table 1. Clay mineral assemblages at ODP Site 758 and potential source areas.

Table 2. Sr-Nd isotopes of clay-sized sediment at ODP Site 758 and potential source areas.

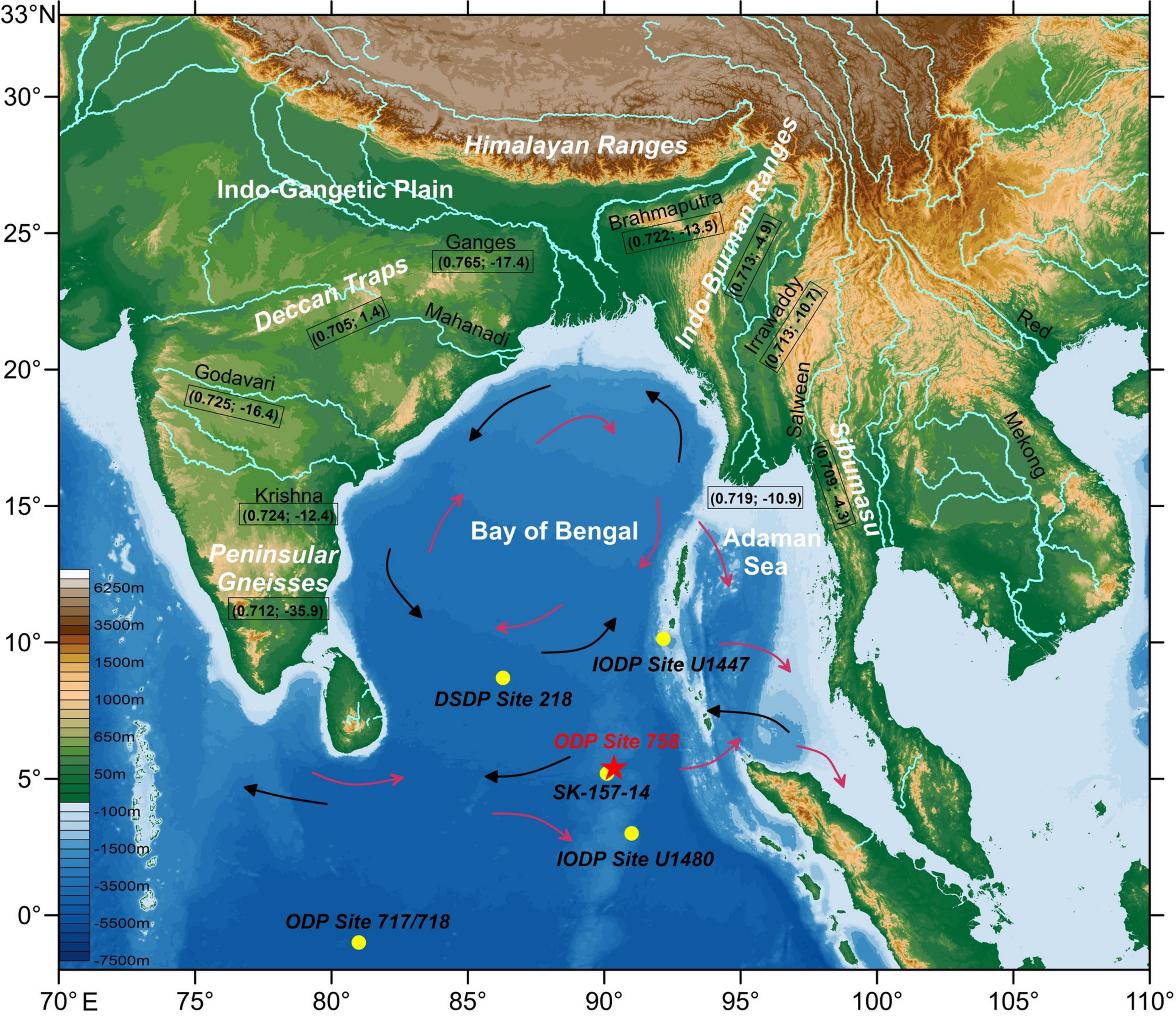
Himalayan Ranges
Indo-Gangetic Plain
Brahmaputra
(0.722; -13.5)
Ganges
(0.765; -17.4)
Deccan Traps
(0.705; 1.4)
Mahanadi
Indo-Burman Ranges
(0.713; -4.9)
Irrawaddy
(0.713; -10.7)
Red
Salween
Sibumasu
(0.709; -4.3)
Mekong
Godavari
(0.725; -16.4)
Krishna
(0.724; -12.4)
Peninsular Gneisses
(0.712; -35.9)
Bay of Bengal
(0.719; -10.9)
Adaman Sea
IODP Site U1447
DSDP Site 218
ODP Site 758
SK-157-14
IODP Site U1480
ODP Site 717/718
6250m
3500m
1500m
1000m
650m
50m
-100m
-1500m
-3500m
-5500m
-7500m
33°N
30°
25°
20°
15°
10°
5°
0°
70° E
75°
80°
85°
90°
95°
100°
105°
110°

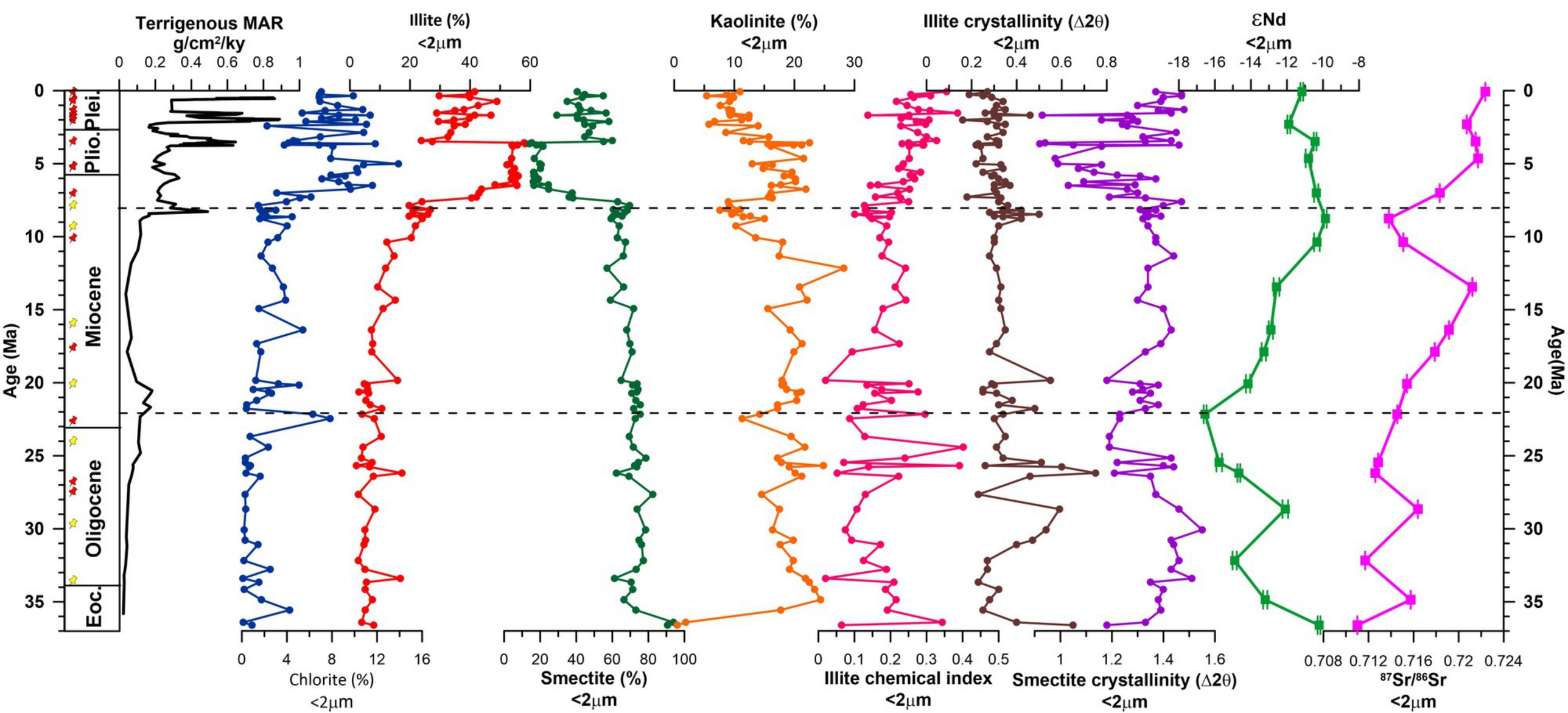
Terrigenous MAR
g/cm²/ky
Illite (%)
<2μm
Kaolinite (%)
<2μm
Illite crystallinity (Δ2θ)
<2μm
εNd
<2μm
Plei.
Plio.
Miocene
Oligocene
Eoc.
Age (Ma)
Age(Ma)
Chlorite (%)
<2μm
Smectite (%)
<2μm
Illite chemical index
<2μm
Smectite crystallinity (Δ2θ)
<2μm
87Sr/86Sr
<2μm

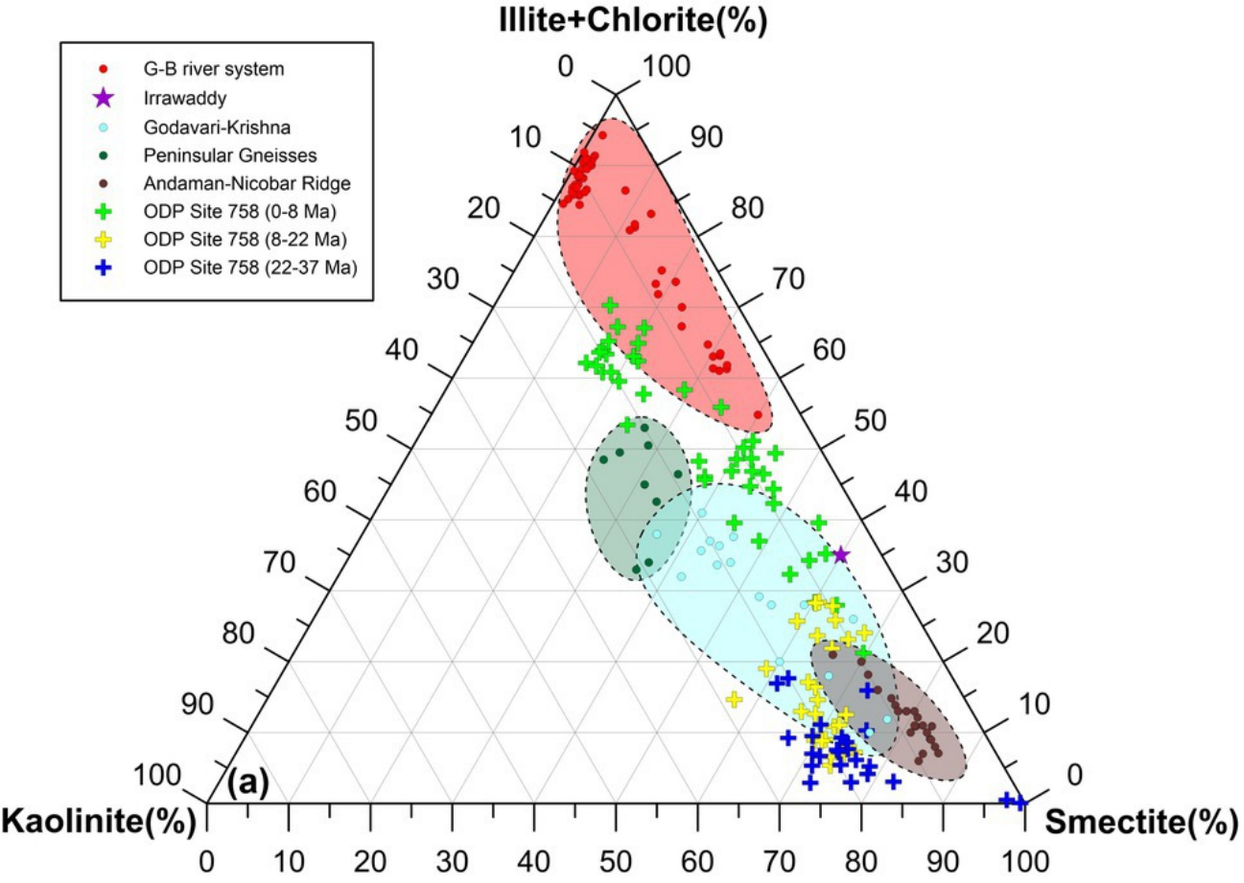
Illite+Chlorite(%)
Kaolinite(%)
Smectite(%)
(a)
G-B river system
Irrawaddy
Godavari-Krishna
Peninsular Gneisses
Andaman-Nicobar Ridge
ODP Site 758 (0-8 Ma)
ODP Site 758 (8-22 Ma)
ODP Site 758 (22-37 Ma)

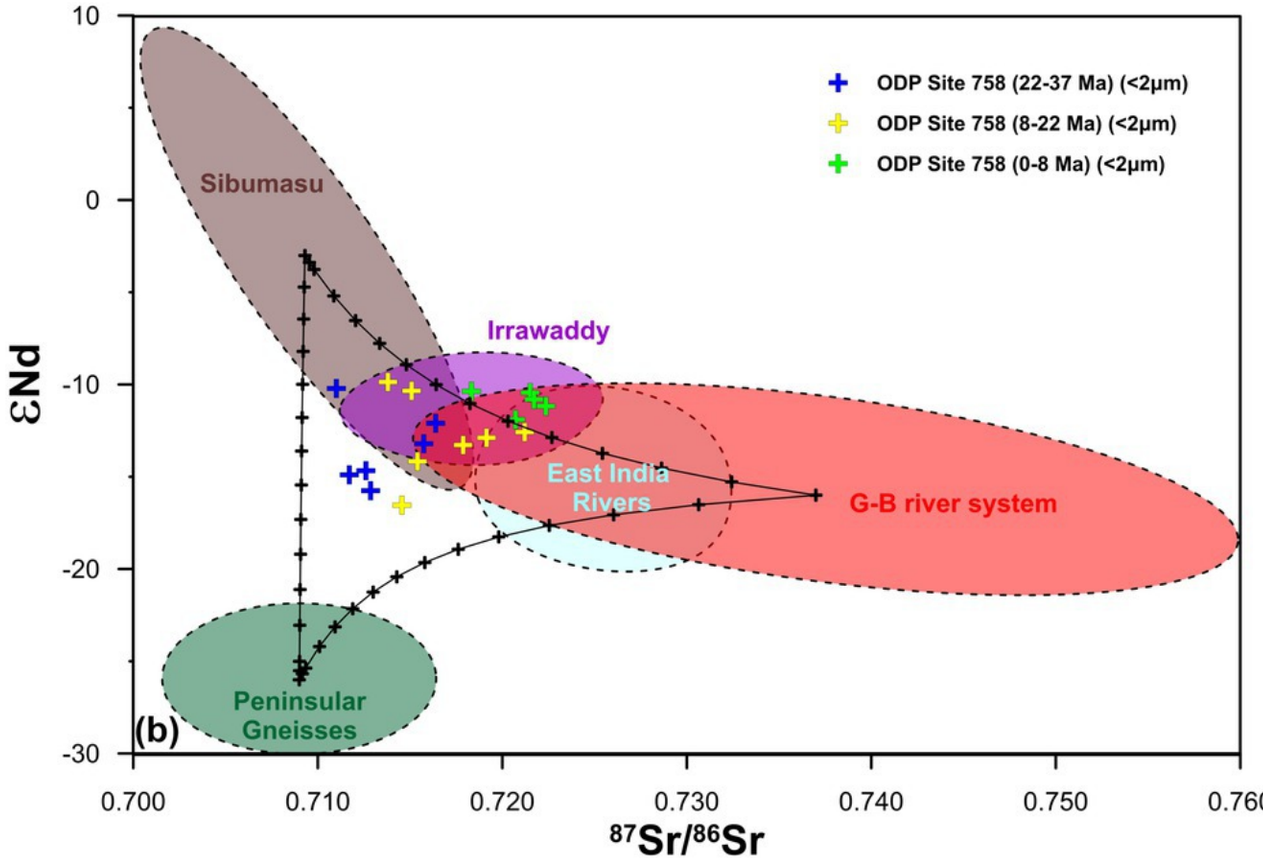
εNd
87Sr/86Sr
(b)
Sibumasu
Irrawaddy
East India Rivers
G-B river system
Peninsular Gneisses
ODP Site 758 (22-37 Ma) (<2μm)
ODP Site 758 (8-22 Ma) (<2μm)
ODP Site 758 (0-8 Ma) (<2μm)

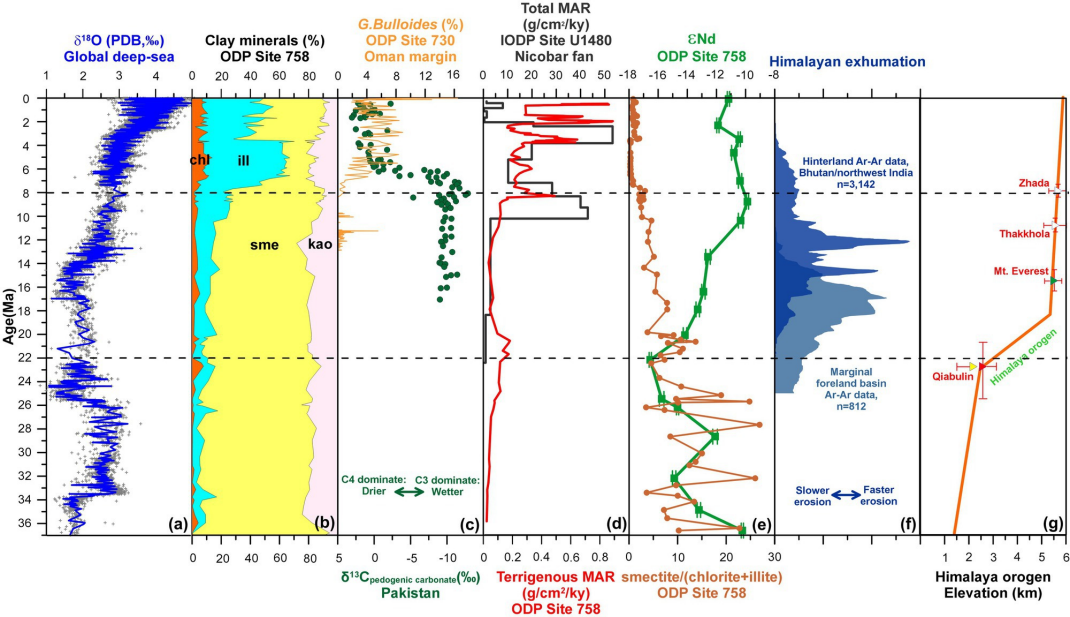
δ18O (PDB,‰)
Global deep-sea
Clay minerals (%)
ODP Site 758
G.Bulloides (%)
ODP Site 730
Oman margin
Total MAR
(g/cm²/ky)
IODP Site U1480
Nicobar fan
εNd
ODP Site 758
Himalayan exhumation
Age(Ma)
chl
ill
sme
kao
(a)
(b)
(c)
(d)
(e)
(f)
(g)
C4 dominate: Drier
C3 dominate: Wetter
Hinterland Ar-Ar data,
Bhutan/northwest India
n=3,142
Marginal
foreland basin
Ar-Ar data,
n=812
Slower erosion
Faster erosion
Zhada
Thakkhola
Mt. Everest
Himalaya orogen
Qiabulin
δ13Cpedogenic carbonate(‰)
Pakistan
Terrigenous MAR
(g/cm²/ky)
ODP Site 758
smectite/(chlorite+illite)
ODP Site 758
Himalaya orogen
Elevation (km)

(a) Late Eocene

Asia
Indochina
Himalaya Orogen
India
Proto-BoB
ODP
Site 758

(b) Early Miocene

Asia
Proto-Tibetan
Plateau
Himalaya Orogen
Indochina
India
Proto-BoB
ODP
Site 758

(c) Late Miocene

Asia
Tibetan Plateau
Himalaya Orogen
Indo-Burman
Ranges
India
Indochina
BoB
ODP
Site 758

(d) At present

Asia
Tibetan Plateau
Himalaya Orogen
Indo-Burman
Ranges
India
Indochina
BoB
ODP
Site 758

Table 1. Clay mineral assemblages of ODP Site 758 and potential source areas.

Samples	Age	Smectite (%)	Illite (%)	Kaolinite (%)	Chlorite (%)	References
ODP Site 758	Average (37-0 Ma)	55	25	16	5	This study
	Average (8-0 Ma)	35	43	14	8	
	Average (22-8 Ma)	67	13	17	2	
	Average (37-22 Ma)	74	7	18	1	
Ganges-Brahmaputra Rivers	Surface sample	15	58	14	13	Rodolfo (1969)
Irrawaddy River	Surface sample	60	15	20	5	
Godavari-Krishna Rivers	Surface sample	53	23	7	18	Phillips et al. (2014)
Peninsular Gneisses	Late Pleistocene-Holocene	31	30	15	24	Kessarkar et al. (2003)
Andaman-Nicobar Ridge	Late Pleistocene-Holocene	79	4	9	9	Ali et al. (2015)

Table 2. Sr-Nd isotopes of clay-sized sediment at ODP Site 758 and potential source areas.

Samples	Depth (m)	Age (Ma)	$^{87}Sr/^{86}Sr$ ($\pm 2\delta \times 10^{-6}$)	$^{143}Nd/^{144}Nd$ ($\pm 2\delta \times 10^{-6}$)	εNd (±2δ)	Reference
ODP Site 758	1.05	0.07	0.722362 ± 4	0.512065 ± 4	-11.18	This study
	34.71	2.31	0.720719 ± 6	0.512028 ± 4	-11.90	
	44.90	3.48	0.721509 ± 4	0.512103 ± 4	-10.44	
	60.45	4.63	0.721720 ± 8	0.512084 ± 8	-10.81	
	89.58	7.01	0.718324 ± 4	0.512106 ± 6	-10.38	
	115.58	8.77	0.713805 ± 4	0.512132 ± 4	-9.87	
	122.19	10.38	0.715086 ± 6	0.512108 ± 8	-10.34	
	132.00	13.44	0.721215 ± 6	0.511993 ± 8	-12.58	
	141.47	16.39	0.719145 ± 6	0.511977 ± 6	-12.89	
	146.00	17.89	0.717884 ± 6	0.511957 ± 6	-13.28	
	154.20	20.06	0.715411 ± 6	0.511912 ± 6	-14.16	
	180.20	22.16	0.714557 ± 4	0.51179 ± 4	-16.54	
	199.51	25.46	0.712857 ± 4	0.51183 ± 8	-15.76	
	209.20	26.18	0.712604 ± 4	0.511886 ± 4	-14.67	
	216.70	28.65	0.716383 ± 4	0.512018 ± 8	-12.09	
	228.57	32.17	0.711704 ± 6	0.511874 ± 6	-14.90	
	241.21	34.86	0.715746 ± 4	0.511961 ± 6	-13.21	

	248.62	36.60	0.711013 ± 4	0.512114 ± 4	-10.22	
Ganges River	Surface sample		0.764614		-17.37	Singh et al. (2008)
Brahmaputra River	Surface sample		0.722116	0.511934	-13.54	Singh and France-Lanord (2002)
Irrawaddy River	Surface sample		0.713330		-10.70	Colin et al. (1999)
	Surface core		0.719134	0.512082	-10.86	Damodararao et al. (2016)
Godavari-Krishna Rivers	Surface sample		0.724463 ± 22	0.511901 ± 11	-14.38	Ahmad et al. (2009)
Peninsular Gneisses	Gneissic Rock		0.711816 ± 10	0.510799 ± 18	-35.88	Peucat et al. (1989)
Sibumasu	Rock sample		0.708572	0.511305	-4.34	Awasthi and Ray (2020); Chen et al. (2002); Xu et al. (2008)